Available online at www.sciencedirect.com

ScienceDirect

journal homepage: www.elsevier.com/locate/bbe

Original Research Article

Detection of pseudo brain tumors via stacked LSTM neural networks using MR spectroscopy signals

Emre Dandil [a,*], *Semih Karaca* [b]

[a] *Department of Computer Engineering, Faculty of Engineering, Bilecik Seyh Edebali University, Bilecik, Turkey*
[b] *Information Technologies Department, Bilecik Seyh Edebali University, Bilecik, Turkey*

ARTICLE INFO

Article history:
Received 17 September 2020
Received in revised form
19 November 2020
Accepted 6 December 2020
Available online 30 December 2020

Keywords:
Pseudo brain tumors
Magnetic resonance spectroscopy
Classification
Deep learning
LSTM

ABSTRACT

Magnetic resonance spectroscopy (MRS) is one of the non-invasive tools used in the detection of brain tumors. MRS provides a metabolic profile about the brain. In this profile, MRS patterns of the tumors and pseudo tumors can be similar to each other. For this reason, accurate diagnosis and classification of brain tumor is of vital importance for the patient's treatment planning. It has been widely preferred by physicians in recent years because it does not pose the risk of infection and death due to surgery like biopsy. In this study, binary classification of brain tumors and normal brain tissue with pseudo-brain tumors is achieved *via* deep neural networks using MRS data. For the classification of MRS signals, a stacked model based on Long Short-Term Memory (LSTM) and Bidirectional Long Short-Term Memory (Bi-LSTM) deep neural networks is proposed. In the experimental studies in the study, MRS signals from normal brain tissue, brain tumor and pseudo-brain tumors in the INTERPRET database are used. Since the MRS data belonging to a large number of tumors and pseudo-tumors are required for training and testing of the LSTM neural networks, the number of data for the MRS dataset is increased by data augmentation methods. Training and testing of the LSTM neural networks used are performed with a repeated 5-fold cross validation and 10 repetitions for each model. As a result of this study, proposed a stacked model for computer-aided binary classification of MRS data, classification results of 93.44%, 85.56%, 88.33% and 99.23% are obtained for the classification of pseudo brain tumor with glioblastoma, diffuse astrocytoma, metastatic brain tumors and normal brain tissue, respectively. Therefore, it is confirmed that the proposed LSTM-based stacked method is successful in detecting pseudo brain tumors using MRS signals.

1. Introduction

Nowadays, cancer is the second leading cause of human death after cardiovascular diseases [1]. According to the world health organization, 9.1 million people died from cancer in 2018 [2]. Although the brain tumors comprise 2% of all cancers, they are disproportionately responsible for cancer-related deaths [3]. According to the World Cancer Report published by the World Health Organization in 2020, while brain and central nervous

* *Corresponding author at*: Department of Computer Engineering, Faculty of Engineering, Bilecik Seyh Edebali University, 11210, Bilecik, Turkey
E-mail address: emre.dandil@bilecik.edu.tr (E. Dandil).

https://doi.org/10.1016/j.bbe.2020.12.003

system cancers were the 17th most common cancer type in 2018, approximately 297 thousand new cases were recorded worldwide [4].

Clinical findings, radiological imaging and histopathology reports play a significant role in the diagnosis of brain tumors. Magnetic resonance imaging (MRI), which provides anatomical information about the brain, and magnetic resonance spectroscopy (MRS), which provides information of the metabolites in the brain, are non-invasive methods used in the diagnosis of brain tumors. The histopathological analysis of a biopsy is the best method for diagnosis of a brain tumor accurately. However, a biopsy has the risk of mortality since it cannot be carried out in all instances [5,6]. MRI has been used in the clinical setting for the diagnosis of brain tumors since the early 1980s [7]. It also provides the best soft tissue contrast among the imaging methods [8]. However, MRI has low sensitivity and can be misleading in determining the type and grade of the tumor [9]. MRS is a non-invasive technique used in the diagnosis of the brain tumors. It provides metabolic information of the tissue under investigation. MRS is used in determining whether the tumor appears benign or malignant by the diagnosis of the type, grade and aggressiveness of the tumor [10]. While it is not possible to distinguish some tumor types with similar images by using MRI, it can be diagnosed with MRS.

Gliomas are the tumors of the central nervous system tumors. They are divided into four different grades from I to IV by WHO classification according to its histopathological features [11]. Tumors categorized as grade I are usually treated non-operatively and are considered as benign. Although Grade II brain tumors are generally benign, they can also be malignant in some cases. Grade III tumors are mostly malignant. Grade IV tumors are called as glioblastoma multiforme and are the most malignant tumors. Structures that are similar to tumors but are not neoplastic in MRI or some metabolite peaks in MRS signal data are called as pseudo tumors. Classifying a lesion as a pseudo-tumor prevents a possible biopsy and changes the treatment management. Examples of pseudo tumors include abscesses, infectious, ischemic, or demyelinating lesions [12].

Pseudo-tumors are also known as idiopathic intracranial hypertension (IIH), pseudo-tumor cerebri syndrome (PTCS) or benign intracranial hypertension. Pseudo-tumors are neurological syndromes that cause increased intracranial pressure (ICP), headache and vision loss despite they are not a mass lesion, underlying infection or malignant tumor [13]. Pseudo-tumors are the cases where there are no definite focal neurological symptoms or signs and the CSF maintains its normal composition [14]. Therefore, it is difficult to determine the pseudo-tumors. Pseudo-tumors occurs potentially in obese women of childbearing age [15]. The possible diseases and conditions that may be associated with pseudo-tumors include bronchitis, sinusitis, middle ear infections, gastroenteritis, urinary tract infections, HIV infection, Lyme disease and varicella [16]. The causes of pseudo-tumor can be listed as brain edema, osmotic edema, vasogenic edema, increased vascular volume, venous hypertension, and arterial dilatation [17]. Distinguishing real tumor from pseudo-tumor is going to completely change the treatment process to be applied to the patient. For a pseudo-tumor, the process may be limited to laboratory tests, while a biopsy and surgery may be planned for a real tumor. In most cases, it is difficult to distinguish a real tumor from a pseudo-tumor with conventional MRI methods [18]. On the other hand, while the grades of brain tumors can be determined with MR spectroscopy data, real and pseudo tumors can also be distinguished [19].

The diagnosis of pseudo tumors that act as a tumor is vital for the patient and is crucial for the accurate treatment planning. Since visual pattern of pseudo tumor is similar to the real tumor, classification of tumors with MRS data is a task that requires high experience. Therefore, in the clinical evaluation of pseudo brain tumors, the robust and reliable results of the proposed automatic detection are remarkable both in terms of time and detection accuracy. Thus, verification with an automated detection method in making the final decision of cases can consolidate the clinician's confidence and increase the applicability potential to classifiers. When the studies proposed in previous for the detection of brain tumors with the help of MRS signals are examined, it is seen that there are a limited number of several studies in distinguishing pseudo brain tumors from real tumors. The limited number of the studies [20,21] proposed for the detection of pseudo tumors is generally based on the interpretation of the proportional values of metabolites. In addition, it is clear that in the proposed previous studies, stages such as pre-processing feature extraction and selection, classification in the detection of brain tumors using MRS signals were performed by different methods. It is noteworthy that there is no decision support system, a learning-based hybrid system or an approach based on classification proposed in this regard. In this study, an approach is presented to facilitate the work of radiologists doing this task and to provide them with a preliminary idea during the decision-making process. In the study, a method based on stacked LSTM deep neural networks is proposed for computer-aided binary classification of glioblastoma multiforme brain tumors, metastatic brain tumors, diffuse astrocytoma brain tumors, and normal brain tissues with pseudo-brain tumors. As a result of the experimental studies carried out in the study, high accuracy performance is achieved with LSTM and Bi-LSTM deep neural networks. In addition, the binary classification results achieved using the proposed stacked LSTM and Bi-LSTM were compared with the results obtained with 1D-CNN. The next sections of the study are organized as follows: In section two, previously proposed studies on the detection of brain tumors on MRS signals are examined. In section three, the method proposed in this study, magnetic resonance spectroscopy and the dataset used in the study are detailed. In section four, experimental studies are explained, and in section five, the results and discussions are presented. In the last section, a general evaluation of the study is performed and the study is concluded.

2. Related works

When the previous studies are investigated, it is seen that many studies conducted on detection, classification and grading of brain tumors using MRS data. Preliminary studies in the detection of brain tumors on MRS data were generally aimed at monitoring the ratios and changes of metabolites to

each other. In such a study, McBride et al. [22] detected tumors by comparing key metabolites in the MRS spectrum with normal brain tissue. In the study, it was seen that there was significant decreases in the mean peak height ratios of NAA/Cho, NAA/Cr, and significant increases in Cho/Cr. Hourani et al. [23] proposed the differentiation between neoplastic and non-neoplastic brain lesions using the metabolite ratios and intensities obtained from the MRS data by using the discriminant function analysis. Majos et al. [20] proposed a method which is based on the ratios of the metabolites in MRS dataset for differentiating between tumors and pseudo-tumoral lesions in the brain. Weis et al. [24] argued that the use of the difference spectra (DS) would be advantageous in grading brain tumors on MRS data using the correlation analysis of the normalized spectral amplitudes and the standard deviation of the scatter plot points. Kaur et al. [25] designed a method using metabolite ratios and weighting these ratios by the Fisher and the parameter-free bat optimization algorithm to show difference among the tumor grades.

In order to provide the clinical experts for automatic classification and detection of brain tumors on MRS signals, many studies were performed to classify MRS signals. Lisboa et al. [26] evaluated statistical and neural networks methods in nuclear magnetic resonance spectral classification and selection of metabolites. In their study, Butzen et al. [27] proposed a logistic regression (LR) based pattern recognition model for the classification of the brain lesions by using MRS signals. The developed statistical LR model enabled the discrimination of neoplastic and non-neoplastic brain lesions. Devos et al. [5] classified the MRS data of brain tumors using linear discriminant analysis and least squares support vector machines (LS-SVMs). Tate et al. [28] proposed a decision support system for diagnosis and grading of brain tumors. The data acquired from four different centers were clustered according to their pathology by using automated pattern recognition techniques. Arús et al. [29] proposed a web-based decision support system that works with distributed networks for brain tumor detection on MRS data. Georgadis et al. [30] proposed a pattern recognition system by combining the MR image features and MRS metabolite ratios for the discriminating among brain pathologies. The proposed pattern recognition system was designed using the support vector machines classifier with radial basis kernel function. Faria et al. [31] classified the MRS data of the brain tumors by partial least squares discriminant analysis (PLS-DA). Tsolaki et al. [32] used pattern recognition system to process MRS data for differentiation of the brain tumors. For the classification procedure, three datasets were created to find the optimum combination of parameters and discrimination was performed using three machine learning methods as: Naïve-Bayes, support vector machine (SVM) and k-nearest neighbor (*k*-NN). Vicente et al. [33] proposed a method for the classification of brain tumors. In the method, the data is extracted with peak integration method and linear discriminant analysis was applied to produce diagnostic classifiers. In their study, Nachimuthu *and* Baladhandapani [34] proposed an automated pattern recognition method using MRI and MRS data for the diagnosis of brain tumors. In their study, Yang et al. [35] investigated whether dimensionality reduction improves classification of brain tumor on MRS signals using manifold learning and unsupervised clustering when comparing with a linear method. They used Laplacian eigenmaps and independent component analysis for data reduction. Lukas et al. [36] proposed a method for brain tumor classification on long echo MRS data using LS-SVMs. Arizmendi et al. [37] classified the brain tumors using regularized artificial neural networks by combining dimensionality reduction and classification methods with Gaussian decomposition (GD) and variance analysis. Vieira et al. [21] performed binary classification abscesses with brain tumors and healthy subjects tissue using pattern recognition methods on MRS data. Yang et al. [38] applied a method of spectral analysis based on discrete wavelet transform using single voxel MRS signals for clustering of brain tumors. In the study, low grade, high grade and normal brain tissue signal patterns were used with extracting of key features on MRS signals. Crain et al. [39] proposed binary classification method based on metabolite peak height ratios. Depciuch et al. [40] proposed a classification method based on Raman and infrared spectroscopy methods. In the studies, the researchers indicated that principal component analysis (PCA) showed that significance of the chemical changes seen between cancer and control tissues and it was efficient in differentiating the infected tissue from the healthy one.

In recent years, with the advances in deep learning networks, there are also state-of-the-art studies proposed for the detection and classification of brain tumors using various deep neural network methods on MRS signals. Lu et al. [41] detected brain tumors using deep learning methods with data augmentation and distillation on MRS signals. In the study, Dandil [42] proposed a method based on artificial immune systems algorithm for the feature extraction from MRS signals taken from INTERPRET dataset. The classification success of the proposed feature extraction on MRS signals was detected by probabilistic neural networks, extreme learning machines, support vector machines, linear discriminant analysis, *k*-nearest neighbor algorithm and Bayes classification methods. In their study, Dandil *and* Bicer [43] provided automated grading of brain tumors using MRS signals obtained from the INTERPRET database using LSTM deep neural networks. In the study, spectral entropy and instantaneous frequency measurements conducted using MRS signals showed that detection performance increased.

3. Proposed method

The general flow diagram of the system proposed in the study is given in Fig. 1. Firstly, after the brain region of the patient to be imaged is scanned with the MRI machine, MR image and MR spectroscopy are obtained. Then, MR spectroscopy data are first standardized to be used in the LSTM deep neural networks proposed in this study and data augmentation processes are performed. In the last, pseudo brain tumors are detected by binary classification *via* the proposed stacked LSTM networks.

3.1. *Magnetic resonance spectroscopy (^1H MRS)*

MRS uses strong magnetic fields on living tissue. It is aimed to create an energy exchange between this applied external magnetic field and hydrogen (^{1}H), phosphorus (^{31}P) or carbon

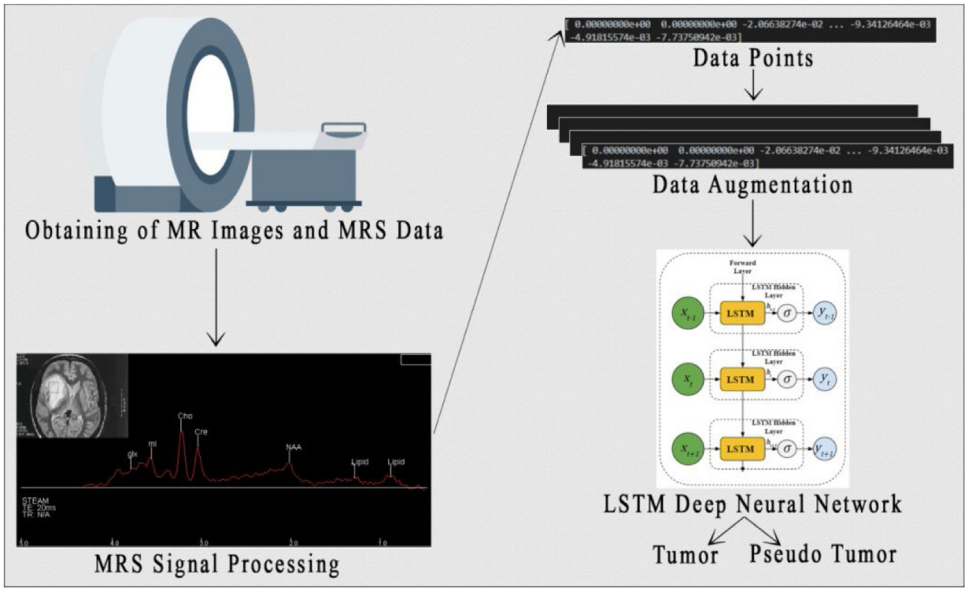

Fig. 1 – General overview of the proposed system for the classification of brain tumors and pseudo brain tumors.

(^{13}C), which are abundant in living tissue. ^{1}H MRS is the most widely used method in clinical practice [44]. As a result, in MRS, a signal is obtained in the frequency domain where different metabolites in the brain peak at different frequency or frequency ranges. While the vertical axis represents the intensity of the signal, the position of the signal in the frequency scale on the horizontal axis is expressed in parts per million (ppm). While the peaks of the metabolites with high density in the brain are large, the peaks of the metabolites with low density are small. The obtained signal provides a measurable profile of tissue metabolism in the brain and facilitates the diagnosis and grading of tumors. In the diagnosis of brain tumors, it is possible to make a diagnosis without biopsy after clinical controls with MRS. With the help of MRS, brain, a sensitive organ, is kept away from the risks posed by surgical operations.

In brain tissue, the main metabolites peaks observed with MR spectroscopy can be listed as *mI* at 3.56 ppm, *Cho* at 3.2 ppm, *Cr* at 3.0 ppm, *NAA* at 2.0 ppm, *Lac* at 1.3 ppm and *Lip* at 0.9 and 1.3 ppm [45]. The increased Cho level in the brain indicates the accelerated membrane production and proliferating brain tumor [46]. Since NAA is found only in neurons and most brain tumors are of non-neuronal origin, it is almost absent in tumor tissue [47]. A preliminary conclusion can be obtained about the type of tumor by comparing different metabolite concentrations such as NAA/Cho, Cho/Cr with each other [48]. Some metabolite peaks observed on MR spectroscopy obtained from the brain tissue of a healthy individual are presented in Fig. 2(a), and of an individual with glioblastoma brain tumor are presented in Fig. 2(b).

MR spectroscopy can be obtained from only a limited brain region as a single voxel or from more than one voxel (multi-voxel). In multi-voxel, MRS is obtained from the brain tissue to be examined and many other regions around it separately. When receiving a single voxel MRS signal, signals from the area outside the selected region of interest are suppressed [49]. Single voxel ^{1}H MRS has a key role in diagnosis of brain tumors by providing additional biochemical information [50]. STEAM and PRESS are the two most commonly used methods in single voxel applications [51]. The density of vibrations applied during the acquisition of the MRS signal is determined by the echo time (TE). While the echo time is relatively longer in employing PRESS, it is shorter on STEAM [52]. Long TE provides information on only Cho, Cr and NAA metabolites, while limited number of peaks facilitates the separation of metabolites in the region of interest. Short TE provides more information about metabolites. The ppm ranges, peak values and some important characteristics of important metabolites observed with short TE time ^{1}H MRS are given in Table 1.

3.2. *MRS dataset*

MRS data used in this study for the diagnosis of pseudo brain tumors were obtained from INTERPRET (International Network for Pattern Recognition of Tumours using Magnetic Resonance) [53,54] dataset. INTERPRET dataset is an EU project conducted with six international centers. The INTERPRET project was developed using the validated brain tumor spectra data with masses and the database is public dataset for both clinical experts and worldwide researchers. The database contains both short TE and long TE MRS signals as single voxel for brain tumors predominantly, pseudo brain tumors and normal brain tissue. The pre-processing protocols of MRS signals with pipeline and all cases included in the validated-database are found in García-Gómez et al. [55] and Julià-Sapé et al. [54], respectively. The purpose of the project can be listed as spreading the use of MRS, enabling radiologists to classify brain tumors using MRS, helping to plan treatment and therapy processes, and making MRS an alternative for biopsy. Within the framework of these purposes, the validated-database consists of 366 short echo single voxel spectra and 304 long echo single voxel spectra in total for brain tumors,

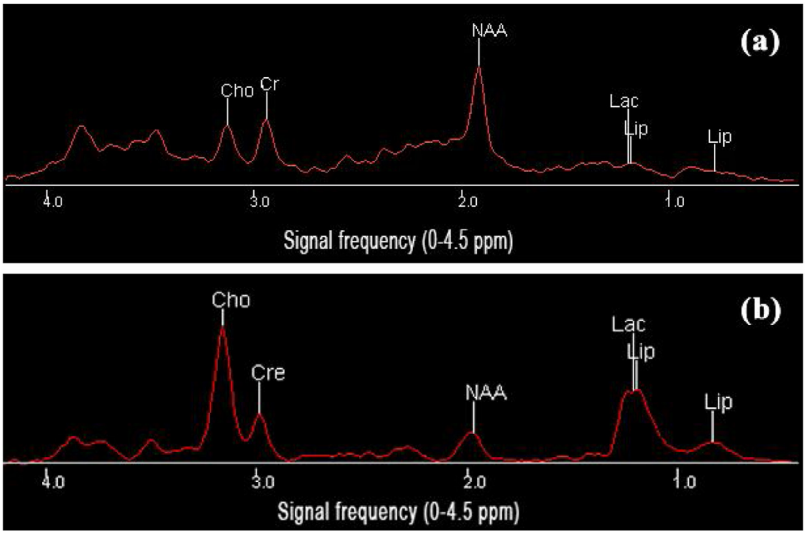

Fig. 2 – (a) MR spectrum of healthy brain tissue; (b) MR spectrum of a patient with glioblastoma brain tumor.

other pathological brain masses and normal brain tissues at 1.5 T PRESS or STEAM [54]. In addition, a decision support system (DSS) software was developed for radiologists to better interpret spectroscopy data. There are few databases where a large number of MRS data belonging to the brain are brought together and made available to researchers. Since short TE spectral signal pattern contain more of information than long TE spectra for metabolites and other compounds, it is considered useful for classification of brain tumors. Hence, in short TE MRS spectra of INTERPRET database, many metabolites are detected such as Cr, Cho, NAA, mI, Gly, taurine, Lac, Ala, glycine, Lip and macromolecules with different ppm values [55]. Therefore, in this study, we created a sub-dataset by the short TE single voxel MRS data of 29 Grade IV glioblastoma multiforme brain tumors, 26 normal brain tissues, 19 metastatic brain tumors, 9 diffuse astrocytoma brain tumors and 9 pseudo-brain tumors from INTERPRET database. It was known that six of the pseudo brain tumors had abscesses. Fig. 3 shows the distribution of the MRS dataset used in this study according to tumor type. In this study, the INTERPRET database was chosen since there are limited conditions that MRS data can be obtained, the database combines various tumor types, and it is still used in current studies.

Fig. 4 shows MR image and MR spectroscopy signals of normal brain tissue. All data points in MRS signals of 26 normal brain tissue samples were averaged separately and normalized after their standard deviations were calculated, which is presented in Fig. 4. As seen in Fig. 4, in MR spectroscopy of normal brain tissue, Cho level is low and NAA level appears to be high since there is no tumor in the brain. Low Cho level and high NAA level, as seen in Fig. 4, are same for all samples. Lac and Lip peaks also have similar signal magnitude for all samples.

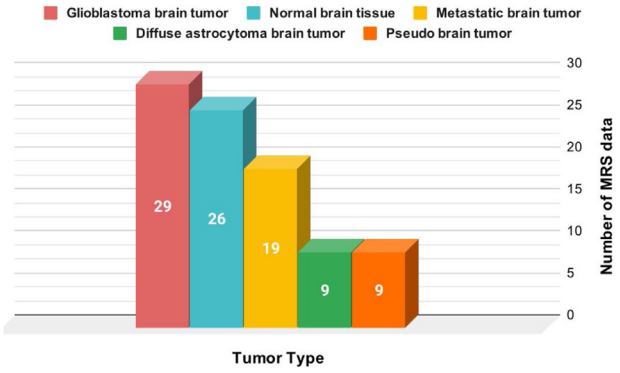

Fig. 3 – Distribution of the MRS dataset used in this study by tumor types.

Table 1 – Peak values and characteristics of key metabolites observed with short TE time MRS.

ppm value	Metabolite	Characteristics
0.9–1.3	lipids (Lip)	disintegration of brain tissue
1.35	lactate (Lac)	anaerobic glucose marker
1.47	alanine (Ala)	occurs in abscess and meningioma
2.02, 2.6	NAA	symptoms of neuron health/neural marker
2.05/2.5	glutamate + glutamine (Glx)	neuro-transmitter
3.02, 3.9	creatine (Cr)	cell metabolism, cell proliferation
3.2	choline (Cho)	cell metabolism, cell proliferation
3.56, 4.06	myo-inositol (ml)	osmotic marker, recommended glial marker

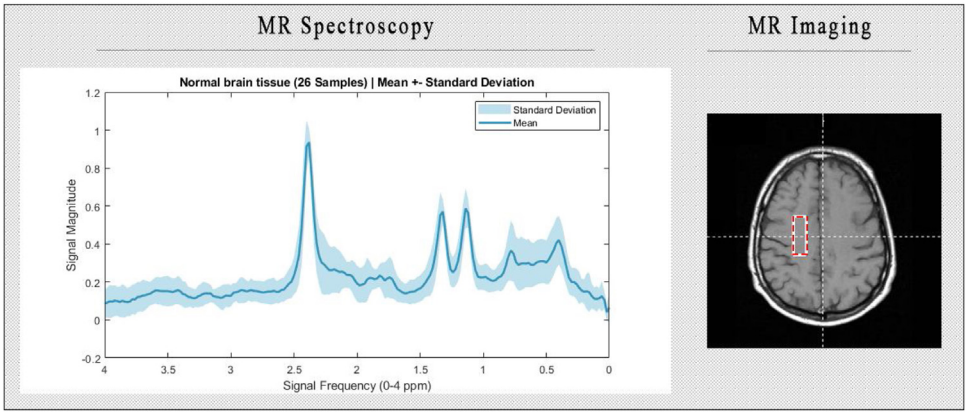

Fig. 4 – Mean and standard deviations of all MR spectroscopy signals of normal brain tissue in dataset and the relevant single voxel of a MR image.

Fig. 5 shows MR spectroscopy signals and MR image of a patient with glioblastoma brain tumor in dataset. All data points in MRS signals of 29 glioblastoma brain tumors samples were averaged separately and normalized after their standard deviations were calculated. Cho peak is found to be high and NAA is found to be low in glioblastoma brain tumor. The high Cho peak and low NAA peak in glioblastoma brain tumor is valid for relatively all samples. Compared to normal brain tumor, the standard deviation is higher in glioblastoma brain tumors and the MRS data of tumors are more diverse.

MR spectroscopy signals and a MR image of metastatic brain tumor in dataset are denoted in Fig. 6. All data points in the MRS signals of 19 metastatic brain tumors were averaged separately and normalized after their standard deviations were calculated, which is shown in Fig. 6. Similar to glioblastoma brain tumor, Cho level is observed to be high and NAA level is observed to be low. High Cho peak and low NAA peak levels in metastatic brain tumor is valid for almost all samples. The standard deviations of metastatic brain tumors in the dataset are the lowest following normal brain tissue. Signal patterns of all metastatic brain tumor samples are close to each other.

MR spectroscopy signals and a MR image of diffuse astrocytoma brain tumor in dataset are denoted Fig. 7. All data points in the MRS signals of 9 diffuse astrocytoma brain tumor samples are averaged separately and normalized after calculating their standard deviations. In this brain tumor, while Cho and NAA levels are low, Lip levels increase at the level of 1.3 ppm. In diffuse astrocytoma brain tumor, Cho and NAA levels are observed to be low and Lip level increased, which is valid for relatively all samples. The standard deviations of diffuse astrocytoma brain tumors in the dataset are relatively low. There is no increase in Cho level in any sample. NAA level is low but higher than glioblastoma and metastatic brain tumors.

Fig. 8 presents MR spectroscopy signals and MR image of the pseudo brain tumors in dataset. All data points in the MRS signals of 9 pseudo brain tumor samples are again averaged separately and normalized after calculating their standard deviations. In the pseudo brain tumors, as seen in Fig. 8, Cho peak is high and NAA is low, as in glioblastoma and metastatic brain tumors. The high Cho peak and the low NAA peak levels is not the same for all samples. Of all the examined samples, the standard deviations of pseudo brain tumors are found to be the highest. Although the increase in Cho level is similar, the signal samples are differed significantly from each other.

As can be seen from the MRS signal patterns given above, the MR spectroscopy of glioblastoma, metastatic and pseudo

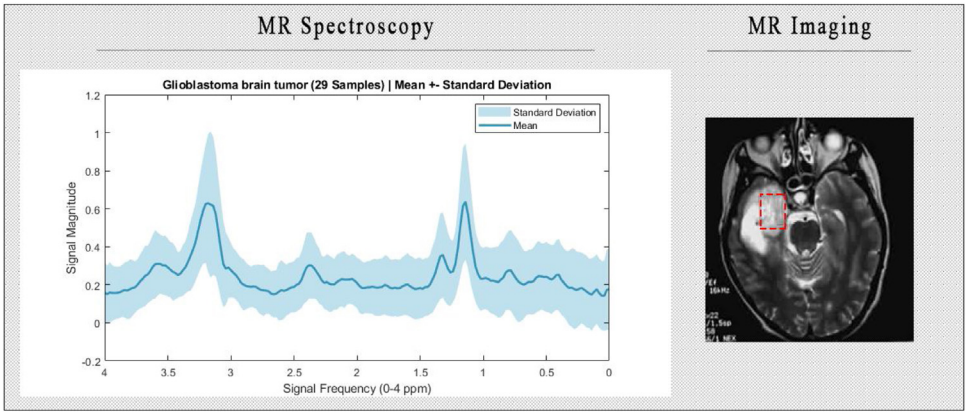

Fig. 5 – Mean and standard deviations of all MR spectroscopy signals of glioblastoma multiforme in dataset and the relevant single voxel of a MR image.

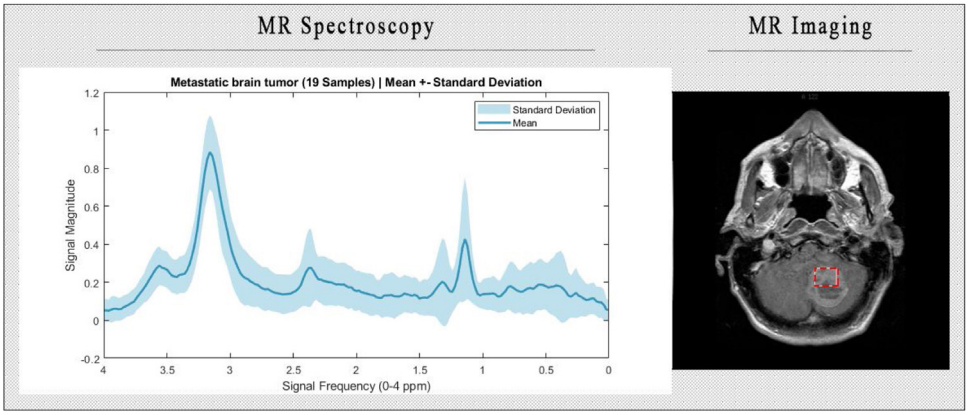

Fig. 6 – Mean and standard deviations of all MR spectroscopy signals of metastatic brain tumors in dataset and the relevant single voxel of a MR image.

brain tumor are similar to each other. For all samples, Cho peak is observed at 3.2 ppm point and NAA peak is observed at 2.0 ppm point. The amount of increased Cho in the brain usually indicates cellular destruction and the presence of a tumor. A low level of NAA also indicates the presence of a tumor.

3.3. *LSTM and Bi-LSTM deep neural networks*

Recurrent neural networks (RNN) are a deep learning algorithms widely used in the analysis of time series. RNN are also used in applications such as natural language processing [56], speech recognition [57], handwriting recognition [58]. In RNN,

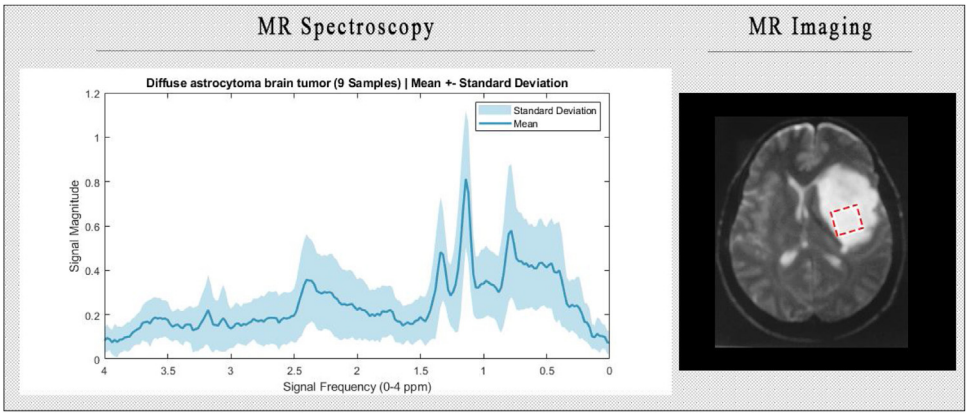

Fig. 7 – Mean and standard deviations of all MR spectroscopy signals of diffuse astrocytoma brain tumors in dataset and the relevant single voxel of a MR image.

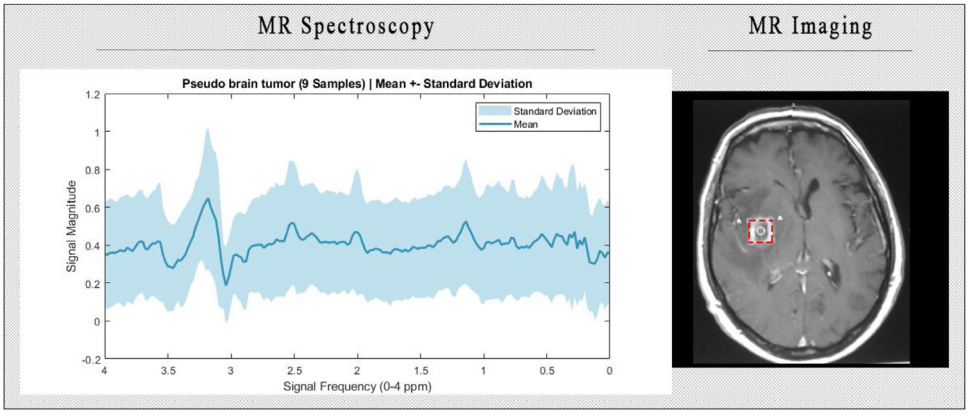

Fig. 8 – Mean and standard deviations of all MR spectroscopy signals of pseudo brain tumors in dataset and the relevant single voxel of a MR image.

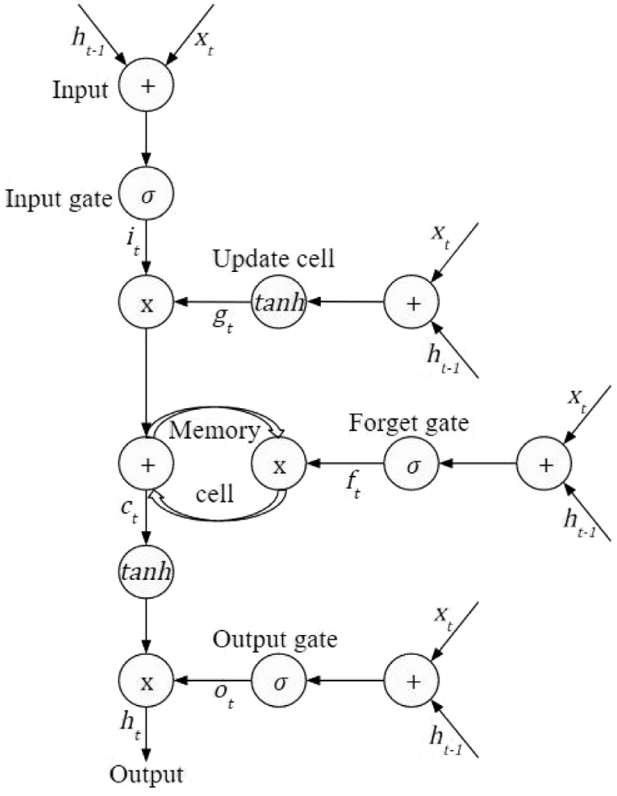

Fig. 9 – Memory cell structure in LSTM deep neural networks.

unlike other feed forward neural networks, the inputs of the network include not only the existing sample but also previous inputs as well. In other words, the stated of *t* is dependent on the information at time *t*-1. RNN was first described in Hopfield networks [59].

Hochreiter *and* Schmidhuber [60], designed long short term memory (LSTM) networks, which is an improved version of RNN, and developed the memory block concept shown in Fig. 9 to solve the vanishing and exploding gradient problem. Memory block enables LSTM cells remember or forget information according to its importance. Information with high importance is used in back propagation, while less important information is forgotten. Bidirectional long short term memory (Bi-LSTM) networks, on the other hand, operate with the logic of training two LSTM networks simultaneously [61]. Two different forms are given as input to the network such as the data and its inverted version with respect to time. Thus, the network keeps information about the future as well as information about the past. The memory block consists of gates as forget gate, input gate and output gate. The equations for the LSTM model are as follows:

$$f_t = \sigma(w_f \cdot [\mathbf{h_{t-1}}, \mathbf{x_t}] + \mathbf{b}_f) \quad (1)$$

$$i_t = \sigma(w_i \cdot [\mathbf{h_{t-1}}, \mathbf{x_t}] + \mathbf{b_i}) \quad (2)$$

$$g_t = tanh(w_g \cdot [\mathbf{h_{t-1}}, \mathbf{x_t}] + \mathbf{b_g}) \quad (3)$$

$$c_t = f_t * c_{t-1} + i_t * g_t \quad (4)$$

$$o_t = \sigma(w_o \cdot [\mathbf{h_{t-1}}, \mathbf{x_t}] + \mathbf{b_o}) \quad (5)$$

$$h_t = o_t * tanh(c_t) \quad (6)$$

The forget gate f_t, the input gate i_t, update state cell g_t and the output gate o_t are presented in Eq. (1), Eq. (2), Eq. (3), Eq. (5), respectively. As the input of these three gates and the update state cell, the previous hidden state h_{t-1} of the previous time step *t*-1, and the current input at time-step x_t are used. While $w_{f,i,g,o}$ is the weight matrices, $b_{f,i,g,o}$ is the bias vector. Memory cell c_t is presented in Eq. (4). The calculation of hidden state of the cell h_t is given in Eq. (6). The sigmoid activation function is shown as σ. Matrix multiplication is represented by "·" and element-by-element matrix multiplication is represented by "*".

General structure for the stacked LSTM and Bi-LSTM networks created in this study is given in Fig. 10. The outputs of the LSTM and Bi-LSTM layers, which are the first layer of the networks, are also taken as input to a LSTM layer. These types of networks are also called as stacked LSTM networks [62].Both networks initially consists of 256-neurons LSTM or Bi-LSTM layer. The input of this layer are samples sized as (5,40) for the LSTM deep neural network. The outputs of this layer are input to a 128 neurons LSTM layer. The outputs of the second LSTM layer are connected to the 64-neurons classical multi-layer perceptron layer. Finally, binary classification is performed by connecting the outputs of the classical layer to the layer with a single classical neuron.

The stacked LSTM and Bi-LSTM deep neural networks models used in this study for detection of pseudo brain tumors are denote in Fig. 11 and Fig. 12, respectively. The outputs of all time steps of the first LSTM layer become inputs to the second LSTM layer. In the second LSTM layer, the regulation method called as dropout is applied. This reduces the over-fitting problem of the model and increases model performance. The output of the second LSTM layer is only taken from the last time step and before classification. The output of second layer

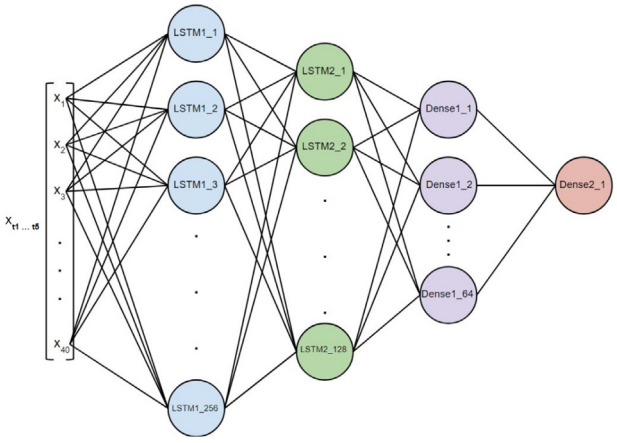

Fig. 10 – General structure of the proposed stacked LSTM deep neural network.

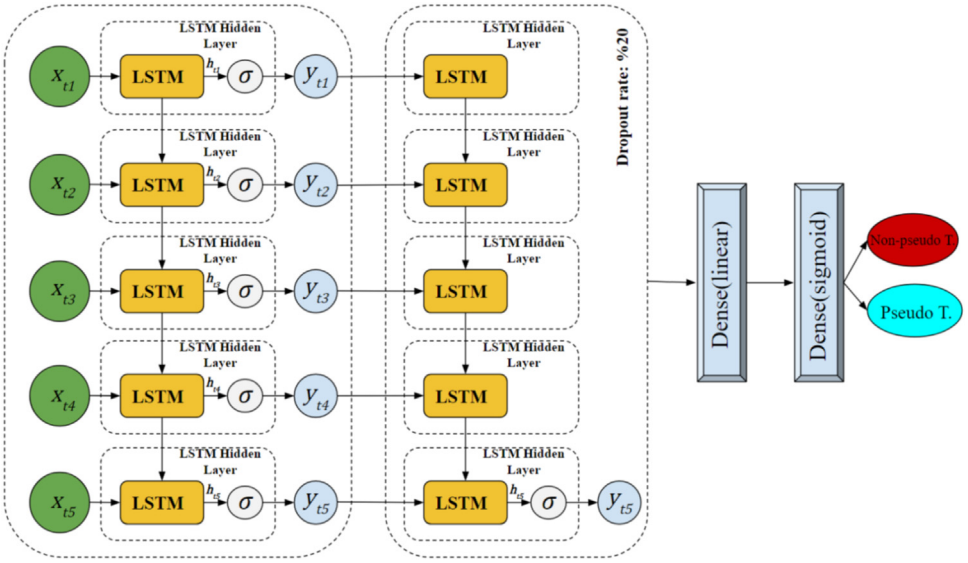

Fig. 11 – Stacked LSTM deep neural network model proposed in this study for the detection of pseudo brain tumors.

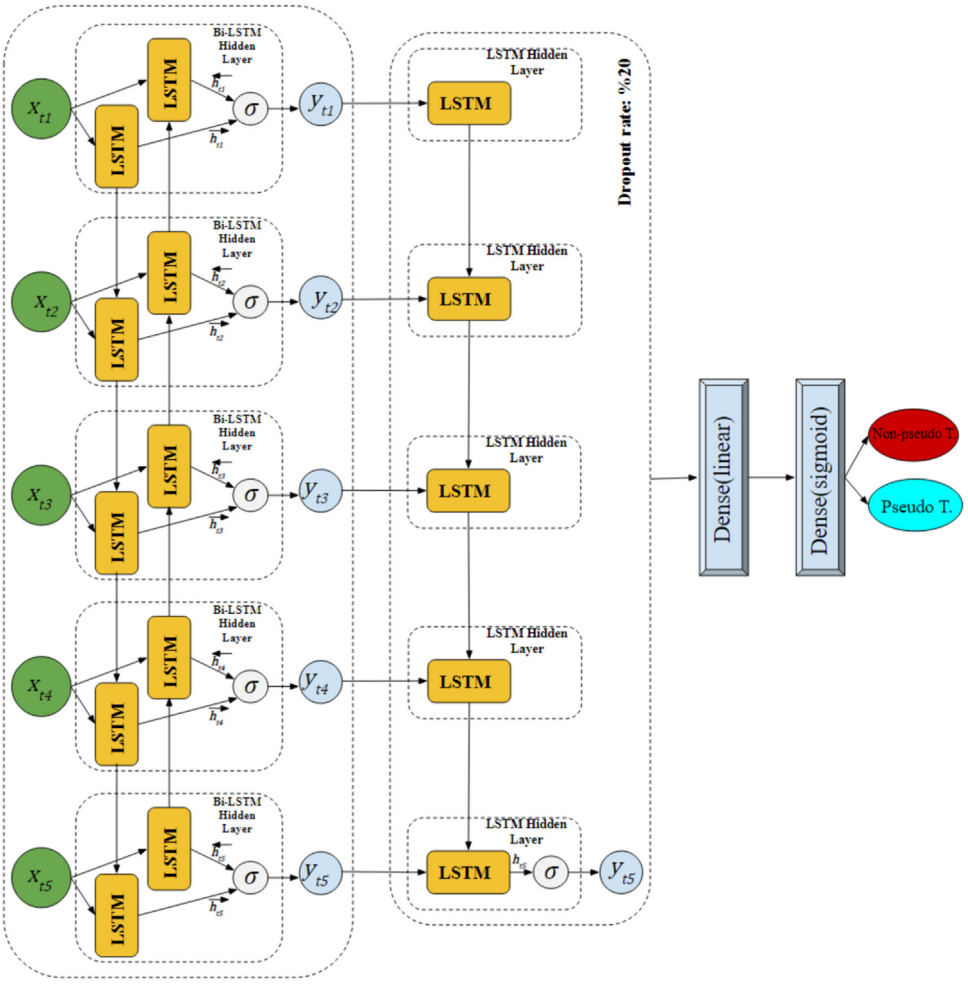

Fig. 12 – Stacked Bi-LSTM deep neural network model proposed in this study for the detection of pseudo brain tumors.

is sent to a classical neural network layer to better learn and increase the number of trainable parameters. The outputs of this layer are input to the last classical neural network whose activation function is sigmoid, and a binary classification is conducted. In the LSTM network, the network has only information about the past. On the other hand, in the Bi-LSTM network, it is aimed to have information about both the past and the future. Since Bi-LSTM networks have two way flow of information, they have the potential to better understand the problem. The first LSTM layer of the LSTM and Bi-LSTM deep neural networks in the proposed study was created in a way to make class predictions in all time steps of the network. Due to the $[y_{t1}, y_{t2}, y_{t3}, y_{t4}, y_{t5}]$ outputs obtained from the first layer of the network, LSTM networks can be designed as stacked and added consecutively.

4. Experimental results

In this study, we present a method on MRS signals based on stacked LSTM and Bi-LSTM deep neural networks for computer-aided binary discrimination of pseudo-brain tumors with glioblastoma multiforme, metastatic, diffuse astrocytoma and normal brain tissues. Besides, the results achieved *via* the proposed stacked LSTM and Bi-LSTM were compared with the results obtained using 1D-CNN architecture. The complete architecture of 1D-CNN is shown in Fig. 13 for comparing the obtained classification results in the proposed stacked LSTM deep neural networks.

Experimental studies in this study was conducted on a computer running Windows 10 operating system with Intel i7-4790k processor (CPU), 8GB memory and NVDIA GeForce GTX 970 graphics card (GPU). The applications were developed by Python programming language. Tensorflow machine learning library was used with Keras, a high level neural network API, to make the machine learning easier. GPU support for Tensorflow was provided by the CUDA Toolkit and CuDNN SDK.

In this study, MRS data of 29 Grade IV glioblastoma brain tumors, 26 normal brain tissues, 19 metastatic brain tumors, 9 diffuse astrocytoma brain tumors, and 9 pseudo brain tumors obtained from INTERPRET dataset were used for detection of pseudo tumors. All classes in the dataset were separately classified as binary with pseudo brain tumors using stacked LSTM and Bi-LSTM deep neural networks. The flow diagram of a classification procedure is shown in Fig. 14. The steps of the study are as follows:

1 Importing MRS data and separating them by labels
2 Using data augmentation techniques
3 Data normalization
4 Resizing data according to the LSTM network
5 Application of variable based (3,4,5) fold cross-validation and 10 repetition process
6 Creation of stacked LSTM and Bi-LSTM deep neural networks
7 Training the models and completing test procedures
8 Getting the average accuracy scores of all cross validations.

MR data of each patient are vectors consisting of 200 data points and a label. After the data is imported, a matrix of size (sample number *x* 201) was created. 201st column of each row contains label information of MRS signal. This label information is removed from the matrix since creating a sample-length vector and labels are encoded as 0 or 1. As a result, the size of the data matrix is (number of samples *x* 200). After the data was imported, it was randomly shuffled within itself. A seed of randomness is used to make these random operations in practice reproducible.

Due to the limited number of pseudo tumors samples in the dataset used in this study, and in order for both classes for

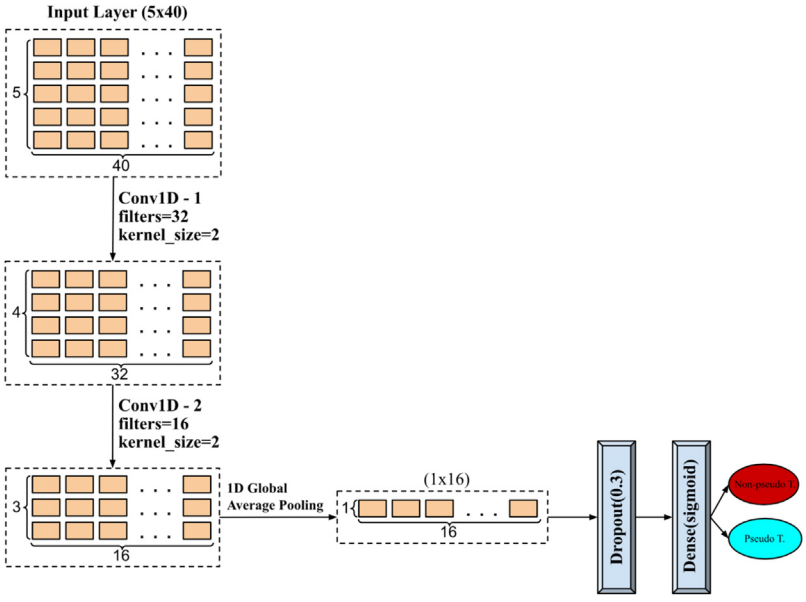

Fig. 13 – The 1D-CNN architecture for comparing the obtained classification results in the proposed stacked LSTM deep neural networks.

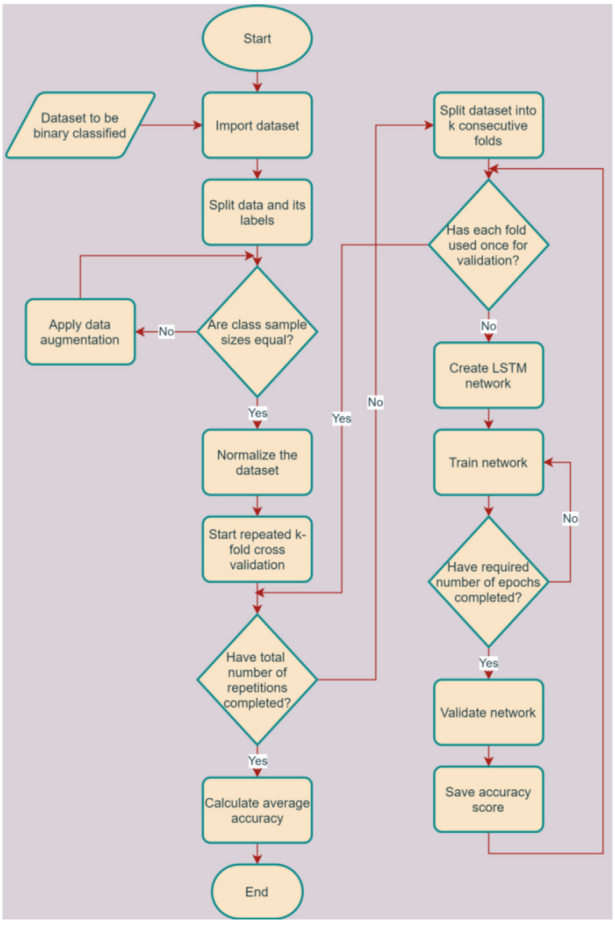

Fig. 14 – Flowchart of the proposed approach to classify pseudo brain tumors with brain tumors using MRS signals.

binary classification to have the same number of samples initially, data augmentation method was applied to the pseudo brain tumor signals. Therefore, the number of pseudo brain tumor data was increased to 29 in the binary classification with glioblastoma, 19 in the classification with metastatic brain tumors, and 26 in the classification with normal brain tissue. Since the number of data is equal in binary classification with diffuse astrocytoma, data augmentation process was not applied. For data augmentation, random values (1 × 200 size) drawn from the normal (Gaussian) distribution are multiplied with the samples to be replicated and new values are generated. The probability density function of the Gaussian distribution is given in Eq. (7).

$$p(x) = \frac{1}{\sigma\sqrt{2}} e^{-\frac{1}{2}\left(\frac{x-\mu}{\sigma}\right)^2} \tag{7}$$

where μ is the mean and σ is the standard deviation. While $\mu = 1$ was used for data augmentation, random values by σ= (0.1,0.2,0.3) were obtained from 3 different distributions. By multiplying these values with the 9 × 200 size pseudo-tumor matrix, a 36 × 200 size dataset was obtained, with the original pseudo tumor data primarily. From this dataset, pseudo tumor data were obtained according to the size of the binary classification and used in next stages. The normal distribution function reaches 0.607 times its maximum at x-σ and x+σ points [63]. For this reason, the points obtained from the normal distribution are closer to the mean value μ. The histogram of the random 200 points obtained from the distribution formed by taking $\mu = 1$ and $\sigma = 0.1$ is shown in Fig. 15 (a). It is seen that the values taken from the distribution are close to the mean value. This indicates that during the data augmentation process, the values of the data are close to the original data. In Fig. 15 (b), the original version of the initial pseudo tumor sample ($\sigma = 0.0$) and the augmented versions ($\sigma = 0.1$, 0.2, 0.3) obtained using this method are plotted on each other. As can be seen in Fig. 15 (b), the values of the data were not far away from the sample during the augmentation process.

After the sample numbers in dataset were applied equal for binary classification, normalization process was realized on the data. For normalization, the method known as ℓ^2 norm or least-squares, which is frequently preferred in machine learning problems, was used. After normalization, a unit vector was obtained where the sum of the squares of all the elements in the vector is 1. Provided that $x=(x_1, x_2, x_3)$, ℓ^2-norm of v vector was calculated as denoted in Eq. (8) and normalized as in Eq. (9). This normalization process can be carried out for each sample or for each feature. This application was conducted for each sample.

$$||x||_2 = \sqrt{\sum_{k=1}^{n} x_k^2} \tag{8}$$

$$x\_norm = x/||x||_2 \tag{9}$$

The obtained data was resized to fit the stacked LSTM deep neural network structure. For one sample, it was resized to include 200 one-dimensional data points (features), 5 time steps and 40 features per step. Fig. 16 shows the resizing process for a single sample. During this resizing step, it was utilized from the peak integration method [5,25,55], which is used to feature extraction from MRS data and measure major metabolite peaks in certain regions. The separation of major metabolite peaks into 5 different time steps was conducted with the aim of remembering and forgetting these peaks according to their effect on the classification result with the LSTM deep neural network.

In this study, cross validation process was also performed to use all samples in the dataset during training and testing stages for the proposed stacked LSTM network. In this process, known as k-fold, the samples in the dataset are split into k groups with approximately the same number of samples. k-1 groups are used for the training, and the rest of the group is used for the test. By this cross validation process, all groups in the dataset split into k groups are used for both training and testing [64]. In this study, verification was performed by selecting different number fold according to the size of dataset for binary classification. Cross validations were repeated 10 times, enabling different selection of training and test data in each repetition. For example, in the 58 sample data where glioblastoma *vs.* pseudo brain tumor were compared, a 5-fold cross-validation was performed and how training and test

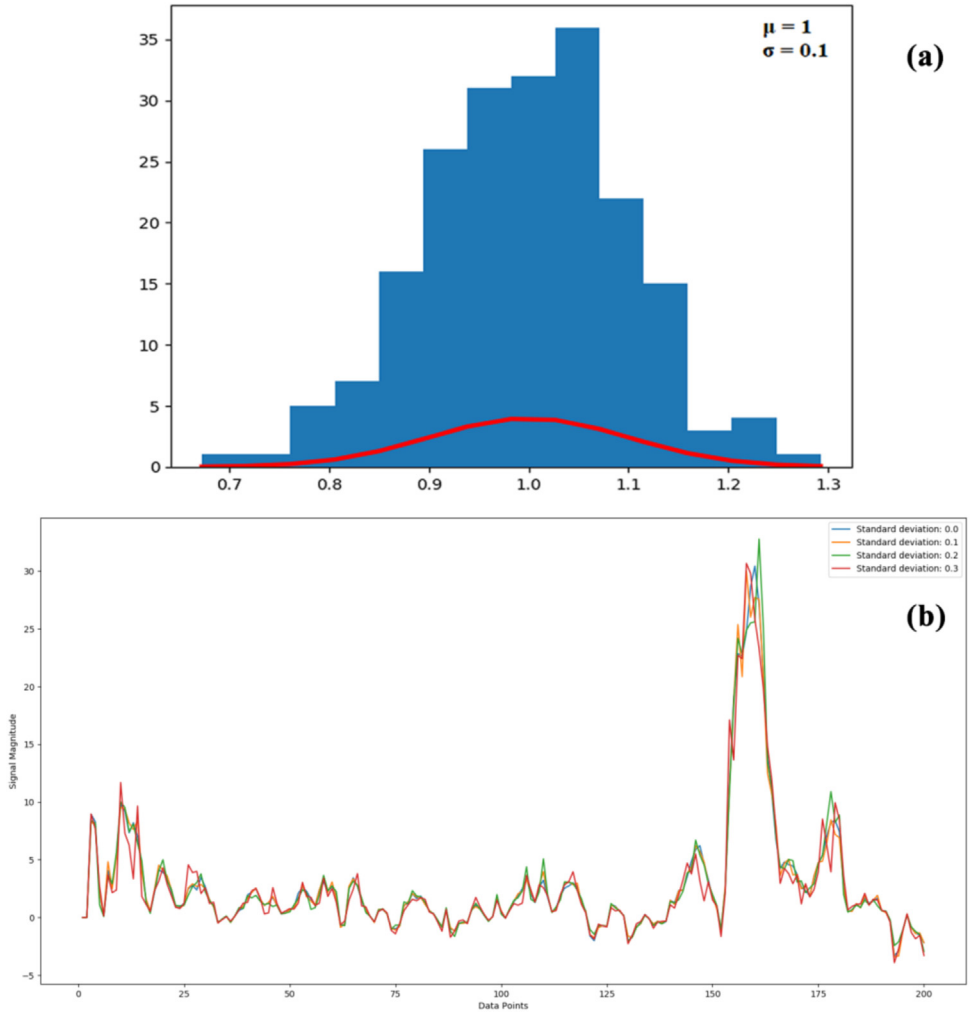

Fig. 15 – (a) Histogram of 200 random points derived from normal distribution; (b) data augmentation procedure to MRS signals of pseudo brain tumors at different standard deviation values.

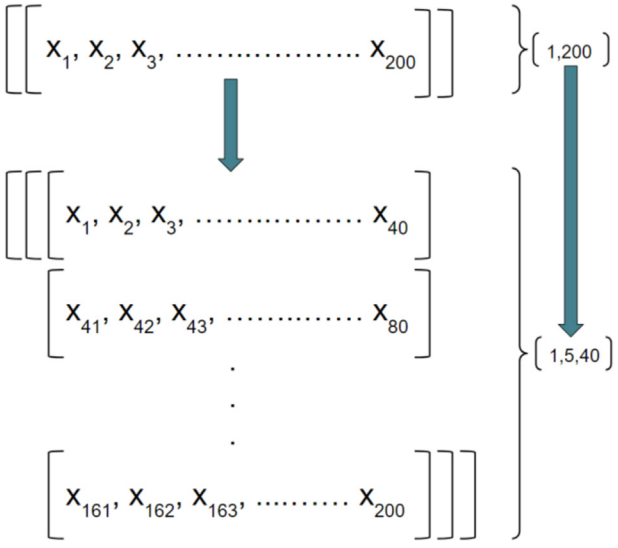

Fig. 16 – Data resizing process to fit the stacked LSTM deep neural network.

data were separated for each validation iteration is shown in Fig. 17. There are approximately 46 training and 12 test samples for each cross validation iteration. With cross validation, the samples in the dataset are split in 50 different ways, then each data is trained and tested. The number of data in total, the number of selected fold value and the number of repetitions in total for binary classifications are given in Table 2.

The kernel and recurrent activation functions, dropout rate and stateful used in the first and second of the stacked LSTM layers are given in Table 3. In the LSTM layer used in the study, the activation of the update state cell g_t is *tanh* and outputs between -1 and 1.The activations of forget gate f_t, input gate i_t and output gate o_t are sigmoid and give outputs between 0 and 1. The dropout rate was used as 20% only in the second LSTM layer. This means that 20% of the inputs of the second LSTM layer will be randomly deprived of activation functions and weight updates. The dropout method is a regularization method which reduces the overfitting problem of the network and improves the model's performance. The stateful feature

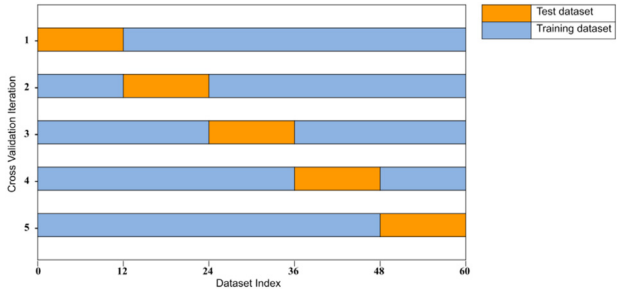

Fig. 17 – 5-fold cross validation in glioblastoma *vs.* pseudo brain tumors for binary classification.

can be explained by the following example: In a network that processes one sample at a time and the weight is updated (batch_size = 1.0), the LSTM neuron saves the output of the last time step after completing all time steps, and that output is in the initial state while the next sample is processed.

In LSTM deep neural networks, weights are called kernels, recurrent kernel and bias. Kernel weights can be defined as the weights of the inputs of the network to all neurons in the LSTM layer. To give an example for the first layer of the network, our network inputs were resized in a way to be 5 time steps and 40 features in each step. Since there are 4 different activation functions in each LSTM neuron in the first layer, the 40 features in each time step have separate weights for these activations. Since there are 256 LSTM neurons in the first layer, their kernel weights can be defined as (40x(256*4))=(40 × 1014). Recurrent kernel is defined as the weights of hidden layers. It is the weight of the hidden LSTM outputs in the previous time step *(t-1)* to all the hidden LSTM neurons in the next time step. Since there are 256 LSTM neurons in the first layer, there are 256 outputs in the previous time step. The weights of these outputs to each LSTM neuron with 4 different activations in the next time step will be (256(256*4))=(256 × 1014). The bias values connected to each of the 4 different activations of each LSTM neuron can be calculated as (4 × 256). Table 4 shows the sizes of weight matrices, which are trainable parameters for the first LSTM layer with 256 neurons.

The model was trained with 25 epochs for each cross validation. During the training and testing, the weights of the stacked LSTM deep neural network were updated after each sample. In other words, the number of samples taken at one time (batch size) is 1.0. This is called stochastic gradient descent (SGD) [65]. The number of samples processed to update the weights of the network can be either a part of the total number of samples (mini-batch) or the whole (batch). Under normal conditions, the SGD method is used in trainings with a large number of data, when all the weights do not fit into memory and to accelerate the training. However, the number of samples processed at one time should always be the same during training and testing, as the first LSTM layer of the deep neural network structure proposed in the study has the stateful feature. The number of samples to be processed at one time (batch size) was taken as 1.0, since the data split for cross validation was of different size for each classified group. Training progresses using 1D-CNN, stacked LSTM and stacked Bi-LSTM in binary classification of pseudo brain tumors with

Table 2 – The number of data in total, the number of selected fold value and the number of repetitions in total for binary classifications.

	Binary classifications			
	glioblastoma *vs.* pseudo tumor	normal tissue *vs.* pseudo tumor	metastatic tumor *vs.* pseudo tumor	diffuse astrocytoma *vs.* pseudo tumor
Number of data in total	58 (29 + 29)	52 (26 + 26)	38 (19 + 19)	18 (9 + 9)
k fold value	5	4	5	3
Number of repetition	10	10	10	10
Number of repetition for each data	50	40	50	30

Table 3 – LSTM network arguments for binary classifications.

	LSTM_1 layer (256)	*LSTM_2* layer (128)
Activation function	hyperbolic tangent (*tanh*)	hyperbolic tangent (*tanh*)
Recurrent activation function	sigmoidal (*sigmoid*)	sigmoidal (*sigmoid*)
Dropout rate	0%	20%
Stateful	available	unavailable

Table 4 – Trainable parameter numbers for the stacked LSTM networks.

Equation number	Weights (kernel: W_x)	Weights (recurrent kernel: W_h)	bias (b)	Total
(1)	W_{xf} : (40,256)	W_{hf} : (256,256)	b_f : (256,)	76,032
(2)	W_{xi} : (40,256)	W_{hi} : (256,256)	b_i: (256,)	76,032
(3)	W_{xg} : (40,256)	W_{hg} : (256,256)	b_g: (256,)	76,032
(4)	W_{xo} : (40,256)	W_{ho} : (256,256)	b_o: (256,)	76,032
Total	W_x : (401,024)	W_h : (2,561,024)	b: (1024,)	304,128

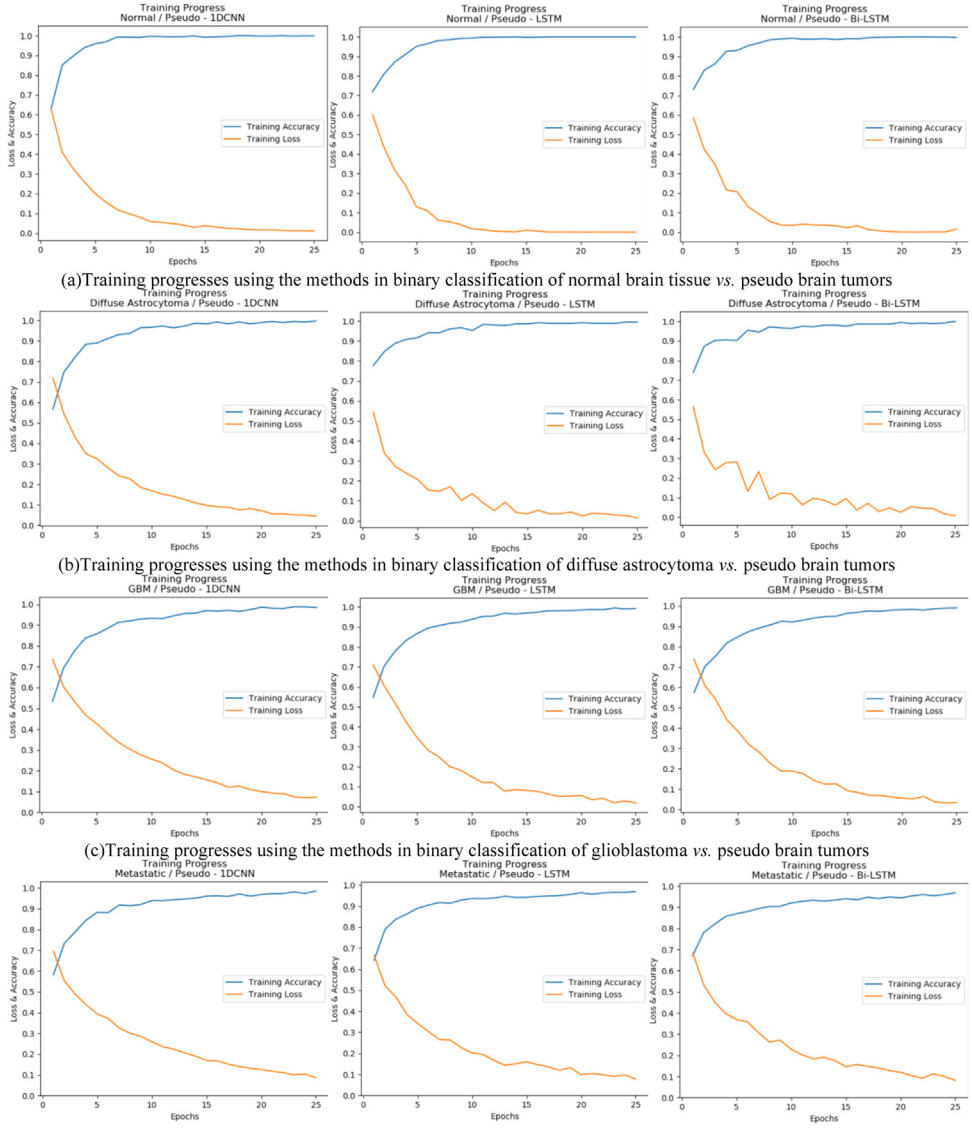

Fig. 18 – Training progresses using 1D-CNN, stacked LSTM and stacked Bi-LSTM in binary classification of: (a) normal brain tissue *vs.* pseudo brain tumors; (b) diffuse astrocytoma *vs.* pseudo brain tumors; (c) glioblastoma *vs.* pseudo brain tumors; (d) metastatic *vs.* pseudo brain tumors.

normal brain tissue, diffuse astrocytoma, glioblastoma and metastatic brain tumors are denoted in Fig. 18. In fact, we determined the completion of the number of epoch as stopping criteria in our study. However, if the training of the network continues unchanged for a certain period of time and no major changes in the loss value begin to occur, the stop criterion is also applied.

5. Results and discussion

After the processes of importing data, data augmentation, normalization, resizing data and creation of LSTM networks were conducted, training and tests were carried out with the split samples. The model was trained with 25 epochs for each cross validation and the model accuracy was calculated with test data. Overall accuracy was taken as the mean of all cross validation accuracies. Input and output dimensions in each layer and the number of trainable parameters for the stacked LSTM, the stacked Bi-LSTM and 1D-CNN models are given in Table 5, Table 6 and Table 7, respectively.

After conducting all the recurrent trainings and tests, the mean and standard deviations of the obtained accuracy, sensitivity and specificity values were calculated. Pseudo brain tumor was taken as positive (1), while other brain tumors and normal brain tissue were taken as negative (0) for accuracy, sensitivity and specificity calculations during binary classifications. These values are calculated with the numbers of True Positive (TP), True Negative (TN), False Positive (FP) and False Negative (FN). TP represents tumors which are actually pseudo

Table 5 – Details of input, output and trainable parameters for the stacked LSTM model.

Layer	Input dimension	Output dimension	Number of trainable parameters
input	-	(1,5,40)	-
LSTM (256)	(1,5,40)	(1,5,256)	304128
LSTM (128)	(1,5,256)	(1,128)	197120
Dense (64)	(1,128)	(1,64)	8256
Dense (1)	(1,64)	(1,1)	65
		Total	509569

Table 6. Details of input, output and trainable parameters for the stacked Bi-LSTM model

Layer	Input dimension	Output dimension	Number of trainable parameters
input	-	(1,5,40)	-
LSTM (256)	(1,5,40)	(1,5,512)	608256
LSTM (128)	(1,5,512)	(1,128)	328192
Dense (64)	(1,128)	(1,64)	8256
Dense (1)	(1,64)	(1,1)	65
		Total	944769

Table 7. Details of input, output and trainable parameters for 1D-CNN model

Layer	Input Dimension	Output Dimension	Number of trainable parameters
Input	-	(1,5,40)	-
Conv1D(32,2)	(1,5,40)	(1,4,32)	2592
Conv1D(16,2)	(1,4,32)	(1,3,16)	1040
GlobalAveragePooling1D	(1,3,16)	(1,16)	0
Dropout(0.3)	(1,16)	(1,16)	0
Dense(1)	(1,16)	(1,1)	17
		Total	3649

tumors and classified as pseudo tumors, TN represents tumors which are not actually pseudo tumors and classified as ''not pseudo tumors'', FP represents tumors which are not actually pseudo tumors but classified as a pseudo tumor, FN represents the tumors which are actually pseudo tumors but classified as ''not pseudo tumors.'' Equations used for accuracy (AC), sensitivity (SE) and specifity (SP) are presented below:

$$AC = \frac{TP + TN}{TP + TN + FP + FN}$$

$$SE = \frac{TP}{TP + FN}$$

$$SP = \frac{TN}{TN + FP}$$

The number of training samples and the number of test samples were applied as 10-fold for all samples in the binary classification group and were presented as the sum of the k-fold cross validation with the determined numbers. The AC value was calculated in all cross validation steps and the mean and standard deviation of all calculated AC values are given. SE and SP values were calculated over the total classification numbers obtained after all cross validation steps were completed. The confusion matrix obtained as a result cross validation of 58 sample GBM brain tumor and pseudo brain tumor classification is given in Table 8. In addition, AC, SE and SP values measured from this confusion matrix are presented in the table. As can be seen from this table, in the binary classification of glioblastoma and pseudo brain tumors, while 93.44% AC value was obtained with stacked LSTM, 92.95% AC value was obtained using stacked Bi-LSTM. Here, it is seen that the stacked LSTM deep neural network is more successful in the binary classification of glioblastoma and pseudo brain tumors. In addition, it is seen from the table that AC, SE and SP values were measured using the 1D-CNN method as 89.13%, 86.56% and 91.72%, respectively. These results are lower than the stacked LSTM and Bi-LSTM methods.

The confusion matrix obtained as a result of binary classification of diffuse astrocytoma brain tumor and pseudo brain tumor with 18 MRS signal patterns in total is denoted in Table 9. As can be seen from Table 9, in the binary classification of diffuse astrocytoma and pseudo brain tumors, while 82.78% AC value was obtained with stacked LSTM, 85.56% AC value was obtained using stacked Bi-LSTM. In this experimental study, AC, SE and SP values were obtained using 1D-CNN as 81.11%, 88.89% and 73.33, respectively. Here, it is seen that the stacked Bi-LSTM deep neural network is more successful in the binary classification of diffuse astrocytoma and pseudo brain tumors. In this binary classification, it is seen that there is a lower accuracy

Table 6 – Details of input, output and trainable parameters for the stacked Bi-LSTM model.

Layer	Input dimension	Output dimension	Number of trainable parameters
input	-	(1,5,40)	-
LSTM (256)	(1,5,40)	(1,5,256)	304128
LSTM (128)	(1,5,256)	(1,128)	197120
Dense (64)	(1,128)	(1,64)	8256
Dense (1)	(1,64)	(1,1)	65
		Total	509569

Table 6. Details of input, output and trainable parameters for the stacked Bi-LSTM model

Layer	Input dimension	Output dimension	Number of trainable parameters
input	-	(1,5,40)	-
LSTM (256)	(1,5,40)	(1,5,512)	608256
LSTM (128)	(1,5,512)	(1,128)	328192
Dense (64)	(1,128)	(1,64)	8256
Dense (1)	(1,64)	(1,1)	65
		Total	944769

Table 7. Details of input, output and trainable parameters for 1D-CNN model

Layer	Input Dimension	Output Dimension	Number of trainable parameters
Input	-	(1,5,40)	-
Conv1D(32,2)	(1,5,40)	(1,4,32)	2592
Conv1D(16,2)	(1,4,32)	(1,3,16)	1040
GlobalAveragePooling1D	(1,3,16)	(1,16)	0
Dropout(0.3)	(1,16)	(1,16)	0
Dense(1)	(1,16)	(1,1)	17
		Total	3649

performance in the differentiation of diffuse astrocytoma and pseudo brain tumors compared to other binary classifications. While there may be many different reasons for this, it is thought that the main reason is that the MRS signal patterns of pseudo brain tumor and diffuse astrocytoma brain tumors show more similarity to each other. Besides, the reason for the lower accuracy in the classification of diffuse astrocytoma and pseudo brain tumors may be the following. As compared to the MRS signal pattern of normal brain tissue, the peak value of the NAA (2.02 ppm, 2.6 ppm) metabolite characteristically decreases and the peak value due to the Cho (3.2 ppm) metabolite increases in the presence of tumor. These increases and decreases are less in Grade I and Grade II gliomas than Grade III and Grade IV gliomas [44,66,67]. Thus, due to the low decrease in NAA and the low increase in Cho in diffuse astrocytoma brain tumor, a Grade II glioma type, MRS signal patterns of the pseudo and diffuse astrocytoma brain tumors indicate similarities in terms of the values of NAA and Cho metabolite peaks. As a result, the accuracy may be lower in binary classification of diffuse astrocytoma and pseudo brain tumors compared to other classifications, due to the slight resemblance of MRS signal patterns.

The confusion matrix obtained as a result of binary classification of metastatic brain tumor and pseudo brain tumor is presented in Table 10. In this binary classification procedure, there are 38 MRS signal patterns in total, including 19 MRS signal of metastatic brain tumor and 19 MRS signal pseudo brain tumor. As can be seen from Table 10, in the binary classification of metastatic and pseudo brain tumors, while 88.33% AC value was obtained with stacked LSTM, 87.62% AC value was obtained using stacked Bi-LSTM. In binary classification of metastatic brain tumor with pseudo brain tumor, AC, SE and SP metrics were achieved using 1D-CNN as 84.44%, 85.26% and 83.69%. Here, although the stacked LSTM deep neural network is more successful in the binary classification of metastatic and pseudo brain tumors, it is seen that the obtained results are very close to each other in terms of performance metrics.

The confusion matrix obtained as a result of normal brain tissue and pseudo brain tumor classification is shown in Table 11. In this binary classification procedure, there are 52 MRS signal patterns in total, including 26 MRS signal of normal brain tissue and 26 MRS signal pseudo brain tumor. As can be seen from Table 11, in the binary classification of normal brain tissue and pseudo brain tumors, while 99.23% AC value was obtained with stacked LSTM, 99.62% AC value was obtained using stacked Bi-LSTM. In binary classification of normal brain tissue with pseudo brain tumor, AC, SE and SP metrics were achieved using 1D-CNN as 95.37%, 96.53% and 94.23%. These results are the highest values for 1D-CNN. However, In Table 11, although the stacked Bi-LSTM deep neural network is more successful in the binary classification of normal brain tissue and pseudo brain tumors, it is seen that the obtained results using the stacked LSTM and Bi-LSTM are very close to

Table 7 – Details of input, output and trainable parameters for 1D-CNN model.

Layer	Input dimension	Output dimension	Number of trainable parameters
input	-	(1,5,40)	-
LSTM (256)	(1,5,40)	(1,5,256)	304128
LSTM (128)	(1,5,256)	(1,128)	197120
Dense (64)	(1,128)	(1,64)	8256
Dense (1)	(1,64)	(1,1)	65
		Total	509569

Table 6. Details of input, output and trainable parameters for the stacked Bi-LSTM model

Layer	Input dimension	Output dimension	Number of trainable parameters
input	-	(1,5,40)	-
LSTM (256)	(1,5,40)	(1,5,512)	608256
LSTM (128)	(1,5,512)	(1,128)	328192
Dense (64)	(1,128)	(1,64)	8256
Dense (1)	(1,64)	(1,1)	65
		Total	944769

Table 7. Details of input, output and trainable parameters for 1D-CNN model

Layer	Input Dimension	Output Dimension	Number of trainable parameters
Input	-	(1,5,40)	-
Conv1D(32,2)	(1,5,40)	(1,4,32)	2592
Conv1D(16,2)	(1,4,32)	(1,3,16)	1040
GlobalAveragePooling1D	(1,3,16)	(1,16)	0
Dropout(0.3)	(1,16)	(1,16)	0
Dense(1)	(1,16)	(1,1)	17
		Total	3649

Table 8 – AC, SE and SP results for binary classification of glioblastoma brain tumor with pseudo brain tumor using stacked LSTM, stacked Bi-LSTM and 1D-CNN deep neural network models.

Model	TP	FN	FP	TN	AC (%)	SE (%)	SP (%)
stacked LSTM	258	32	10	280	93.44 (±8.54)	88.97	96.55
stacked Bi-LSTM	263	27	14	276	92.95 (±8.51)	90.69	95.17
1D-CNN	251	39	24	266	89.13 (±8.81)	86.56	91.72

Table 9 – AC, SE and SP results for binary classification of diffuse astrocytoma brain tumor with pseudo brain tumor using stacked LSTM. Stacked Bi-LSTM and 1D-CNN deep neural network models.

Model	TP	FN	FP	TN	AC (%)	SE (%)	SP (%)
stacked LSTM	80	10	21	69	82.78 (±13.25)	88.89	76.67
stacked Bi-LSTM	80	10	16	74	85.56 (±12.72)	88.89	82.22
1D-CNN	80	10	24	66	81.11 (±14.10)	88.89	73.33

Table 10 – AC, SE and SP results for binary classification of metastatic brain tumor with pseudo brain tumor using stacked LSTM, stacked Bi-LSTM and 1D-CNN deep neural network models.

Model	TP	FN	FP	TN	AC (%)	SE (%)	SP (%)
stacked LSTM	163	27	16	174	88.33 (±13.23)	85.79	91.58
stacked Bi-LSTM	159	31	16	174	87.62 (±12.48)	83.16	91.58
1D-CNN	162	28	31	159	84.44(±11.93)	85.26	83.69

Table 11 – AC, SE and SP results for binary classification of normal brain tissue with pseudo brain tumor using stacked LSTM, stacked Bi-LSTM and 1D-CNN deep neural network models.

Model	TP	FN	FP	TN	AC (%)	SE (%)	SP (%)
stacked LSTM	258	2	5	255	98.85 (±4.05)	99.23	98.08
stacked Bi-LSTM	259	1	3	257	99.23 (±3.77)	99.62	98.85
1D-CNN	251	9	15	245	95.37(±6.64)	96.53	94.23

each other in terms of performance metrics. In addition, in this binary classification, the highest classification accuracy results were achieved using both stacked models.

The number of training and test samples may differ for a single epoch since each set with binary classification had different size and different folds were selected for cross validation. The training and test sample numbers are given as the sum of the training and test samples in all epochs. The total numbers in the error matrices are different because the sample numbers of the binary classification and the *k*-cross validation are different. As each sample in the dataset was used for both training and testing by cross validation, the total number of predictions made for any set can be calculated as *(number of sample * k-fold value)*.

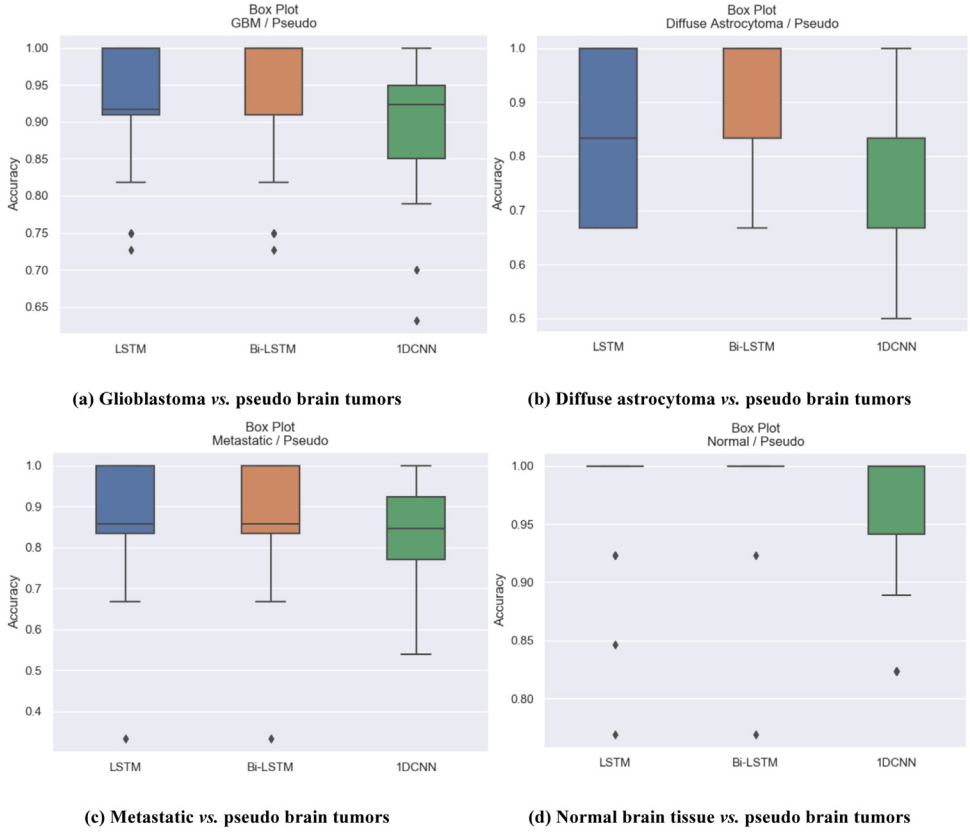

Fig. 19 – The accuracy box plots for binary classification of: (a) glioblastoma *vs.* pseudo brain tumors; (b) diffuse astrocytoma *vs.* pseudo brain tumors; (c) metastatic *vs.* pseudo brain tumors; (d) normal brain tissue *vs.* pseudo brain tumors.

When the test results are examined in experimental studies, it is seen that remarkable AC results were obtained in all set for binary classifications using proposed stacked deep neural networks. The highest AC was obtained in tests of normal brain tissue and pseudo brain tumors classification while the lowest AC was obtained in binary classification for diffuse astrocytoma brain tumor and pseudo brain tumor. The highest SE and SP values for both the stacked deep neural network models were obtained in normal brain tissue and pseudo brain tumor classification. The proposed networks differentiated normal brain tissue from pseudo brain tumor very well. For this classification, the models accurately predicted 259 of 260 pseudo tumor and 255 of 260 normal brain tissues. Moreover, it was observed that the AC values of stacked LSTM and Bi-LSTM models were very close mostly. The accuracy box plots created for the binary classification results of glioblastoma *vs.* pseudo brain tumors, diffuse astrocytoma *vs.* pseudo brain tumors, metastatic *vs.* pseudo brain tumors and metastatic *vs.* pseudo brain tumors using LSTM, Bi-LSTM and 1D-CNN methods are denoted in Fig. 19.

In order to validate the performance of the proposed stacked LSTM method for classification of brain tumors, MRS signals from the diffuse astrocytoma, metastatic, glioblastoma, pseudo brain tumors and normal brain tissue were used by Gradient-weighted Class Activation Mapping (Grad-CAM). Grad-CAM is one of the techniques used to reveal what regions of the input MRS signals are important and functional in brain tumor classification. Grad-CAM denotes the most distinctive regions on the weights of the output layer with convolutional feature maps [68]. As a visualization technique, Grad-CAM is a technology to produce visual explanation for CNN-based classifications uses the gradient of the classification task [69]. In Grad-CAM, a heat map could be created by mapping of important of class weights for feature maps of a convolutional layer. Therefore, the feature map of last convolutional layer obtained using Grad-CAM provides high-level features and spatial information [70]. In Fig. 20, visual comparisons of signals of the envelope MRS spectrum for pseudo brain tumor classification are indicated using Grad-CAM results. Discriminative regions of the MRS signals are highlighted here using brighter colors on Grad-CAM figures. Thus, we use the Grad-CAM to visualize the gradient of the results to denote effectiveness of the stacked LSTM networks for binary classification of pseudo brain tumors on MRS signals.

It is seen that there are similar studies proposed previously for the detection of brain tumors on MRS data. In these studies, many different methods such as tumor classification, feature extraction and selection, tumor differentiation, tumor staging were proposed using various algorithms. Although some of these studies conducted experimental studies on the same dataset, some detected brain tumors on their own dataset. However, since the collection and preparation of MRS data requires quite long and difficult clinical and radiological processes, it is seen in most of the studies that experimental studies are carried out on INTERPRET, a valid and reliable

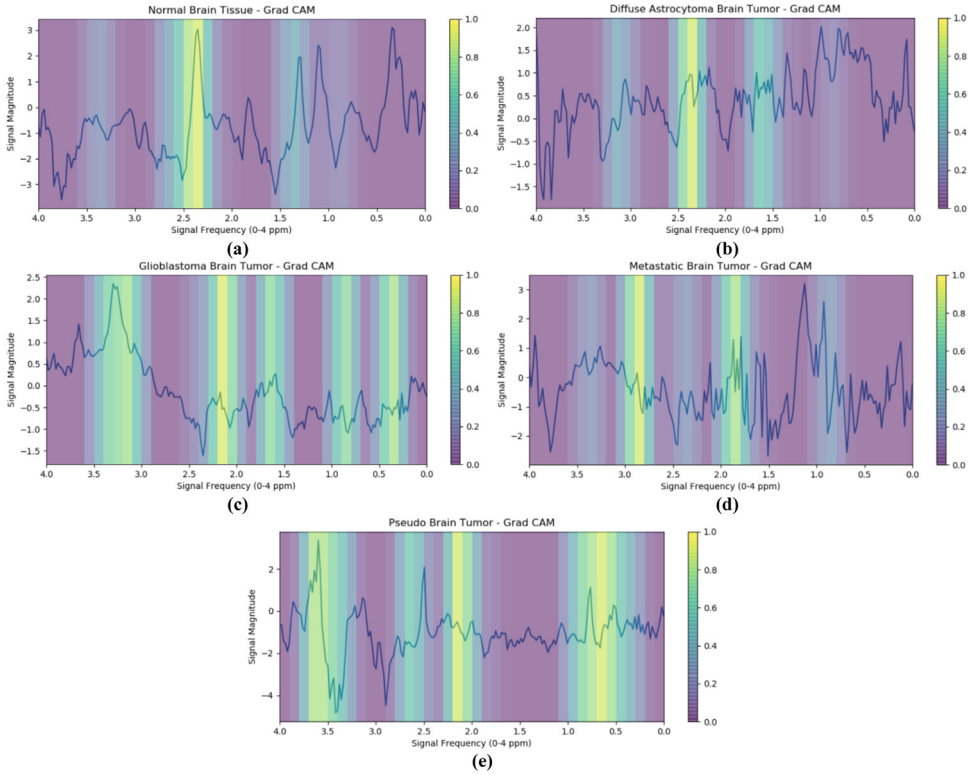

Fig. 20 – Visual Grad-CAM comparisons of MRS signals for pseudo brain tumor classification. Grad- CAM of: (a) normal brain tissue; (b) diffuse astrocytoma brain tumor; (c) glioblastoma brain tumor; (d) metastatic brain tumor; (e) pseudo brain tumor.

Table 12 – Comparison of similar works previously proposed for the detection of brain tumors on MRS data.

Previous study	Dataset	Method	Algorithms	AC (%)
Majós et al. (2004) [71]	INTERPRET	tumor classification	linear LS-SVM	94.00
Devos et al. (2004) [5]	INTERPRET	tumor classification	LS-SVM, LDA	87.30
Lukas et al. (2004) [36]	INTERPRET	tumor classification	LS-SVM, LDA	97.81
Tate et al. (2006) [28]	INTERPRET	tumor diagnosis and grading	a decision support system based pattern recognition	89.00
Luts et al. (2007) [72]	INTERPRET	tumor classification	LS-SVMs	99.73
González-Navarro and Belanche-Muñoz (2009) [73]	INTERPRET	tumor classification, feature selection	radial basis kernel function based SVM (rSVM)	91.00 (±0.05)
Dimou et al. (2009) [74]	their own dataset	tumor classification	SVM	85.00
Majós et al. (2009) [20]	their own dataset	differentiation of tumor and pseudo tumor	metabolite ratio based classifiers	82.00
García-Gómez et al. (2009) [55]	INTERPRET, eTUMOUR	tumor classification	LDA, SVM, LS-SVM, multi-layer perceptron, *k*-NN	90.00
Weis et al. (2010) [24]	INTERPRET	tumor grading	correlation analysis and mean difference spectra	NA
Lu et al. (2013) [75]	their own dataset	tumor classification	SVM + linear discriminant analysis (LDA)	96.67
Wang et al. (2015) [76]	their own dataset	tumor grading	LS-SVM + LDA	98.63
Vieira et al. (2017) [21]	INTERPRET	differentiation of tumor and abscess	random forest + SVM	98.9
Kaur et al. (2018) [25]	their own dataset	tumor grading	Fisher and bat optimization algorithm + *k*-NN	93.72
Dandil (2020) [42]	INTERPRET	feature extraction, tumor classification	extreme learning machine, Bayes, SVM, probabilistic neural network, *k*-NN, LDA	100 (normal *vs.* tumor), 98.58 (low grade *vs.* high grade), 98.94 (primary *vs.* metastasis)
Dandil and Biçer (2020) [43]	INTERPRET	tumor grading	LSTM	98.20
Proposed study	INTERPRET	pseudo brain tumor detection	stacked LSTM and Bi-LSTM	99.23 (±3.77)

NA: not available.

Table 13 – Runtime spent on CPU and GPU in binary classifications for stacked LSTM, stacked Bi-LSTM and 1D-CNN deep neural networks in seconds (*n = number of data*).

	Binary classifications			
	glioblastoma *vs.* pseudo tumor ($n = 58$)	normal tissue *vs.* pseudo tumor ($n = 52$)	metastatic tumor *vs.* pseudo tumor ($n = 38$)	diffuse astrocytoma *vs.* pseudo tumor ($n = 18$)
stacked LSTM *on CPU*	610.21	628.35	703.59	131.96
stacked Bi-LSTM *on CPU*	1203.16	1125.97	1276.51	248.32
1D-CNN *on* CPU	290.84	298.65	335.98	62.41
stacked LSTM *on GPU*	601.53	600.95	676.35	141.10
stacked Bi-LSTM *on GPU*	947.27	944.29	1085.30	209.29
1D-CNN *on* GPU	230.23	224.85	240.41	34.35

database. In Table 12, the highest AC values obtained in some studies conducted on computer aided brain tumor classification in previous on MRS signal data. As can be seen in Table 12, the detection method proposed in this study achieved a high accuracy value for detection pseudo brain tumors. As in this study, when the studies conducted INTERPRET dataset are examined, it is seen that the similar AC results are obtained for detection of brain tumors on MRS data.

The execution times of the training and tests carried out in this study on the processor and GPU according to each set of binary classification are given in seconds in Table 13. When the run-time spent for the tests on the GPU and CPU were examined, it was seen that the GPU times were less on average. In some cases, the same test seemed to spend less time on CPU. In the training of the network, the number of samples processed at once (batch size) was taken as 1 and the number of samples in the sets used was low, so the parallelism and speed advantages provided by the graphics processor could not be utilized much. The GPU provided a more significant advantage in the training of the stacked LSTM networks that were bi-directional and had more data when comparing with the stacked Bi-LSTM. Bi-LSTM network is more suitable for parallelism since data in Bi-LSTM networks is given to two LSTM networks simultaneously, as one straight and one reverse. In addition, in Table 13, processing times are calculated lower in experimental works using the 1D-CNN method. The reason for this is that the 1D-CNN network structure is simpler than the structure of RNN-based stacked LSTM networks and the total number of parameters used in 1D-CNN is less. In general, the CPU in the system does not provide as much parallelism as the GPU; however, it is better than a GPU at a single core speed. In addition, GPU is an integrated system and it is above the RAM. For this reason, RAM bandwidth is high. The number of data that can be memorized at one time is high and the data is easier to move between the RAM and the graphics processor.

6. Conclusion

In this study, computer aided detection of pseudo brain tumors was provided by using both stacked LSTM and Bi-LSTM deep neural networks. Moreover, the achieved binary classification results obtained using stacked LSTM and Bi-LSTM methods were compared with the performance results obtained using 1D-CNN. High accuracy performances was achieved as a result of binary classification of MRS for normal brain tissue, glioblastoma, metastatic and diffuse astrocytoma brain tumors *vs.* pseudo brain tumor. The accuracy results obtained in the study are as follows: 93.44% using stacked LSTM for glioblastoma *vs.* pseudo brain tumor classification, 85.56% using stacked Bi-LSTM for the classification of diffuse astrocytoma *vs.* pseudo brain tumors, 88.33% using stacked LSTM for metastatic *vs.* pseudo brain tumor classification, 99.23% using stacked Bi-LSTM for normal brain tissue *vs.* pseudo brain tumor classification.

In the study, although the number of trainable parameters for the stacked Bi-LSTM model was twice as much as the LSTM network, the difference between the achieved accuracies was very small and also lower accuracy results were obtained in some binary classifications. In the stacked Bi-LSTM model, as a result of using the inverse of the MRS signal for the training of the network, it was observed that the information the network for the following did not affect learning much. Since the data are divided by different combinations many times for training and testing, the obtained results show the accuracy of not only one set, but many sets, that is, the accuracy of the applied models.

The deep neural network models used in the study were tested with structures formed by connecting LSTM and Bi-LSTM layers within themselves or with each other in a layered structure. However, no significant increase in the accuracy values reached was observed. On the other hand, classical neural network structures connected to the front or the end of LSTM and Bi-LSTM layers did not provide an increase in classification accuracy. The parameters of the stacked LSTM and classical neural network layers used in the model were tested in different ways and the model was tried to be optimized to fit all sets. Furthermore, in experimental studies, evaluations for the binary classification of brain tumor on MRS signals using 1D-CNN were also carried out, but it was observed that these results were not more successful than the results achieved *via* the proposed stacked LSTM and Bi-LSTM in any binary classification.

Working with a large number of samples in training and testing deep neural networks is important in terms of obtaining realistic network learning. Thousands of sample data for training or test can be used in classical deep neural network training. However, it is not easy to apply this to MRS signal data. Creating a dataset with MRS signals is difficult to obtain and there are few available dataset in public. In this study, the number of MRS signal samples in the INTERPRET

dataset for the pseudo brain tumor, all other tumor and normal tissue types used for binary classification was very less. Therefore, data augmentation method was used since the number of data of the pseudo brain tumor was especially less than the others. Data augmentation can also be done by copying existing data. However, in this study, MRS data was reproduced using a random procedure without much differentiation in order to obtain unique and different data. As a result, it was confirmed by experimental studies that data augmentation improved the detection accuracy of pseudo brain tumors.

In the future studies, artificial data can be obtained by using different methods alone or together for augmentation of MRS data. In addition, more successful classification results can be achieved by fine-tuning the parameters of the used network. For tumor classification, a model that may be created by combining CNN and LSTM networks for better results. Moreover, the accuracy of the method proposed within the scope of this study can be evaluated with the creation of a new MRS dataset or with other existing MRS datasets.

Compliance with ethical standards

Human and animal rights

The paper does not contain any studies with human participants or animals performed by any of the authors.

Informed consent

Informed consent is obtained from all individual participants included in the study.

Conflict of interest

The author declares that we have no conflict of interest.

Acknowledgements

In this study, we would like to thank all the stakeholders of the project, especially Dr. Margarida Julià-Sapé, for allowing the use of MRS data in the INTERPRET database.

REFERENCES

[1] Fitzmaurice C, Allen C, Barber RM, Barregard L, Bhutta ZA, Brenner H, et al. Global, regional, and national cancer incidence, mortality, years of life lost, years lived with disability, and disability-adjusted life-years for 32 cancer groups, 1990 to 2015: a systematic analysis for the global burden of disease study. JAMA Oncol 2017;3:524–48.

[2] WHO. WHO - Cancer;Accessed from: https://www.who.int/news-room/fact-sheets/detail/cancer2018.

[3] Neugut AI, Sackstein P, Hillyer GC, Jacobson JS, Bruce J, Lassman AB, et al. Magnetic resonance imaging-based screening for asymptomatic brain tumors: a review. Oncologist 2019;24:375–84.

[4] Wild C, Weiderpass E, Stewart B. World cancer report: cancer research for cancer prevention. Lyon: International Agency for Research on Cancer; 2020.

[5] Devos A, Lukas L, Suykens J, Vanhamme L, Tate A, Howe F, et al. Classification of brain tumours using short echo time 1H MR spectra. J Magn Reson 2004;170:164–75.

[6] Yang G, Raschke F, Barrick TR, Howe FA. Nonlinear laplacian eigenmaps dimension reduction of in-vivo magnetic resonance spectroscopic imaging analysis. International Society for Magnetic Resonance in Medicine (ISMRM). 2013. p. 1967.

[7] Ladd ME, Bachert P, Meyerspeer M, Moser E, Nagel AM, Norris DG, et al. Pros and cons of ultra-high-field MRI/MRS for human application. Prog Nucl Magn Reson Spectrosc 2018;109:1–50.

[8] Soares D, Law M. Magnetic resonance spectroscopy of the brain: review of metabolites and clinical applications. Clin Radiol 2009;64:12–21.

[9] Hekmatnia A, Sabouri M, Ghazavi AH, Far PS, Hekmatnia F, Sofi GJ, et al. Diagnostic value of Magnetic Resonance Spectroscopy (MRS) for detection of Brain Tumors in patients. Med Sci 2019;23:939–45.

[10] Majós C, Alonso J, Aguilera C, Serrallonga M, Pérez-Martín J, Acebes JJ, et al. Proton magnetic resonance spectroscopy (1 H MRS) of human brain tumours: assessment of differences between tumour types and its applicability in brain tumour categorization. Eur Radiol 2003;13:582–91.

[11] Louis DN, Perry A, Reifenberger G, Von Deimling A, Figarella-Branger D, Cavenee WK, et al. The 2016 World Health Organization classification of tumors of the central nervous system: a summary. Acta Neuropathol 2016;131:803–20.

[12] Horská A, Barker PB. Imaging of brain tumors: MR spectroscopy and metabolic imaging. Neuroimaging Clin N Am 2010;20:293–310.

[13] Burkett JG, Ailani J. An up to date review of pseudotumor cerebri syndrome. Curr Neurol Neurosci Rep 2018;18:1–7.

[14] Katz VL, Peterson R, Cefalo RC. Pseudotumor cerebri and pregnancy. Am J Perinatol 1989;6:442–5.

[15] Celebisoy N, Secil Y, Akyürekli Ö. Pseudotumor cerebri: etiological factors, presenting features and prognosis in the western part of Turkey. Acta Neurol Scand 2002;106:367–70.

[16] Tasdemir HA, Dilber C, Totan M, Onder A. Pseudotumor cerebri complicating measles: a case report and literature review. Brain Dev 2006;28:395–7.

[17] Milhorat TH. Classification of the cerebral edemas with reference to hydrocephalus and pseudotumor cerebri. Childs Nerv Syst 1992;8:301–6.

[18] Silva HCA, Callegaro D, Marchiori PE, Scaff M, Tsanaclis A, Maria C. Magnetic resonance imaging in five patients with a tumefactive demyelinating lesion in the central nervous system. Arq Neuropsiquiatr 1999;57:921–6.

[19] Cianfoni A, Niku S, Imbesi S. Metabolite findings in tumefactive demyelinating lesions utilizing short echo time proton magnetic resonance spectroscopy. Am J Neuroradiol 2007;28:272–7.

[20] Majos C, Aguilera C, Alonso J, Julia-Sape M, Castaner S, Sanchez J, et al. Proton MR spectroscopy improves discrimination between tumor and pseudotumoral lesion in solid brain masses. Am J Neuroradiol 2009;30:544–51.

[21] Vieira BH, Santos ACD, Salmon CEG. Pattern recognition of abscesses and brain tumors through MR spectroscopy: comparison of experimental conditions and radiological findings. Res Biomed Eng 2017;33:185–94.

[22] McBride DQ, Miller BL, Nikas DL, Buchthal S, Chang L, Chiang F, et al. Analysis of brain tumors using 1H magnetic resonance spectroscopy. Surg Neurol 1995;44:137–44.
[23] Hourani R, Brant L, Rizk T, Weingart JD, Barker PB, Horská A. Can proton MR spectroscopic and perfusion imaging differentiate between neoplastic and nonneoplastic brain lesions in adults? Am J Neuroradiol 2008;29:366–72.
[24] Weis J, Ring P, Olofsson T, Ortiz-Nieto F, Wikström J. Short echo time MR spectroscopy of brain tumors: grading of cerebral gliomas by correlation analysis of normalized spectral amplitudes. J Magn Reson Imaging 2010;31:39–45.
[25] Kaur T, Saini BS, Gupta S. An optimal spectroscopic feature fusion strategy for MR brain tumor classification using Fisher Criteria and Parameter-Free BAT optimization algorithm. Biocybern Biomed Eng 2018;38:409–24.
[26] Lisboa P, Kirby S, Vellido A, Lee Y, El-Deredy W. Assessment of statistical and neural networks methods in NMR spectral classification and metabolite selection. NMR Biomed 1998;11:225–34.
[27] Butzen J, Prost R, Chetty V, Donahue K, Neppl R, Bowen W, et al. Discrimination between neoplastic and nonneoplastic brain lesions by use of proton MR spectroscopy: the limits of accuracy with a logistic regression model. Am J Neuroradiol 2000;21:1213–9.
[28] Tate AR, Underwood J, Acosta DM, Julià-Sapé M, Majós C, Moreno-Torres À, et al. Development of a decision support system for diagnosis and grading of brain tumours using in vivo magnetic resonance single voxel spectra. NMR Biomed 2006;19:411–34.
[29] Arús C, Celda B, Dasmahaptra S, Dupplaw D, Gonzalez-Velez H, Van Huffel S, et al. On the design of a web-based decision support system for brain tumour diagnosis using distributed agents. 2006 IEEE/WIC/ACM International Conference on Web Intelligence and Intelligent Agent Technology Workshops; 2006. pp. 208–11.
[30] Georgiadis P, Kostopoulos S, Cavouras D, Glotsos D, Kalatzis I, Sifaki K, et al. Quantitative combination of volumetric MR imaging and MR spectroscopy data for the discrimination of meningiomas from metastatic brain tumors by means of pattern recognition. Magn Reson Imaging 2011;29:525–35.
[31] Faria AV, Macedo Jr F, Marsaioli A, Ferreira M, Cendes F. Classification of brain tumor extracts by high resolution ^{1}H MRS using partial least squares discriminant analysis. Braz J Med Biol Res 2011;44:149–64.
[32] Tsolaki E, Svolos P, Kousi E, Kapsalaki E, Fountas K, Theodorou K, et al. Automated differentiation of glioblastomas from intracranial metastases using 3T MR spectroscopic and perfusion data. Int J Comput Assist Radiol Surg 2013;8:751–61.
[33] Vicente J, Fuster-Garcia E, Tortajada S, García-Gómez JM, Davies N, Natarajan K, et al. Accurate classification of childhood brain tumours by in vivo1H MRS–a multi-centre study. Eur J Cancer 2013;49:658–67.
[34] Nachimuthu DS, Baladhandapani A. Multidimensional texture characterization: on analysis for brain tumor tissues using MRS and MRI. J Digit Imaging 2014;27:496–506.
[35] Yang G, Raschke F, Barrick TR, Howe FA. Manifold Learning in MR spectroscopy using nonlinear dimensionality reduction and unsupervised clustering. Magn Reson Med 2015;74:868–78.
[36] Lukas L, Devos A, Suykens JA, Vanhamme L, Howe FA, Majós C, et al. Brain tumor classification based on long echo proton MRS signals. Artif Intell Med 2004;31:73–89.
[37] Arizmendi C, Sierra DA, Vellido A, Romero E. Automated classification of brain tumours from short echo time in vivo MRS data using Gaussian Decomposition and Bayesian Neural Networks. Expert Syst Appl 2014;41:5296–307.
[38] Yang G, Nawaz T, Barrick TR, Howe FA, Slabaugh G. Discrete wavelet transform-based whole-spectral and subspectral analysis for improved brain tumor clustering using single voxel MR spectroscopy. IEEE Trans Biomed Eng 2015;62:2860–6.
[39] Crain ID, Elias PS, Chapple K, Scheck AC, Karis JP, Preul MC. Improving the utility of 1 H-MRS for the differentiation of glioma recurrence from radiation necrosis. J Neurooncol 2017;133:97–105.
[40] Depciuch J, Tolpa B, Witek P, Szmuc K, Kaznowska E, Osuchowski M, et al. Raman and FTIR spectroscopy in determining the chemical changes in healthy brain tissues and glioblastoma tumor tissues. Spectrochim Acta A Mol Biomol Spectrosc 2020;225:1–8.
[41] Lu D, Polomac N, Gacheva I, Hattingen E, Triesch J. Human-expert-Level brain tumor detection using deep learning with data distillation and augmentation. arXiv preprint arXiv:200612285 2020.
[42] Dandil E. aiMRS: a feature extraction method from MRS signals based on artificial immune algorithms for classification of brain tumours. IET Signal Process 2020;14:361–73.
[43] Dandil E, Biçer A. Automatic grading of brain tumours using LSTM neural networks on magnetic resonance spectroscopy signals. IET Image Process 2020;14:167–1979.
[44] Callot V, Galanaud D, Le Fur Y, Confort-Gouny S, Ranjeva J-P, Cozzone PJ. 1H MR spectroscopy of human brain tumours: a practical approach. Eur J Radiol 2008;67:268–74.
[45] Kimura T, Sako K, Gotoh T, Tanaka K, Tanaka T. In vivo single-voxel proton MR spectroscopy in brain lesions with ring-like enhancement. NMR Biomed 2001;14:339–49.
[46] Ramin SL, Tognola WA, Spotti AR. Proton magnetic resonance spectroscopy: clinical applications in patients with brain lesions. Sao Paulo Med J 2003;121:254–9.
[47] Howe FA, Opstad KS. 1H MR spectroscopy of brain tumours and masses. NMR Biomed 2003;16:123–31.
[48] Nagori M, Joshi M. Methods and algorithms for extracting values from MRS graph for brain tumour detection. Ieri Procedia 2013;4:331–6.
[49] Blüml S. Magnetic resonance spectroscopy: basics. MR spectroscopy of pediatric brain disorders. Springer; 2013. p. 11–23.
[50] Yang G, Raschke F, Barrick TR, Howe FA. Classification of brain tumour 1 h mr spectra: extracting features by metabolite quantification or nonlinear manifold learning? 2014 IEEE 11th International Symposium on Biomedical Imaging (ISBI); 2014. pp. 1039–42.
[51] Moonen CT, Kienlin MV, Van Zijl PC, Cohen J, Gillen J, Daly P, et al. Comparison of single-shot localization methods (STEAM and PRESS) for in vivo proton NMR spectroscopy. NMR Biomed 1989;2:201–8.
[52] van der Graaf M. In vivo magnetic resonance spectroscopy: basic methodology and clinical applications. Eur Biophys J 2010;39:527–40.
[53] INTERPRET Consortium. International network for pattern recognition of tumours using magnetic resonance; 2002.
[54] Julià-Sapé M, Acosta D, Mier M, Arùs C, Watson D. A multi-centre, web-accessible and quality control-checked database of in vivo MR spectra of brain tumour patients. Magn Reson Mater Phys Biol Med 2006;19:22–33.
[55] García-Gómez JM, Luts J, Julià-Sapé M, Krooshof P, Tortajada S, Robledo JV, et al. Multiproject–multicenter evaluation of automatic brain tumor classification by magnetic resonance spectroscopy. Magn Reson Mater Phys Biol Med 2009;22:5–18.
[56] Wu Y, Schuster M, Chen Z, Le QV, Norouzi M, Macherey W, et al. Google's neural machine translation system: bridging the gap between human and machine translation. arXiv preprint arXiv:160908144 2016.
[57] Graves A, Mohamed A-R, Hinton G. Speech recognition with deep recurrent neural networks. 2013 IEEE International

Conference on Acoustics, Speech and Signal Processing; 2013. pp. 6645–9.
[58] Zhang X-Y, Xie G-S, Liu C-L, Bengio Y. End-to-end online writer identification with recurrent neural network. IEEE Trans Hum Mach Syst 2016;47:285–92.
[59] Hopfield JJ. Neural networks and physical systems with emergent collective computational abilities. Proc Natl Acad Sci 1982;79:2554–8.
[60] Hochreiter S, Schmidhuber J. Long short-term memory. Neural Comput 1997;9:1735–80.
[61] Schuster M, Paliwal KK. Bidirectional recurrent neural networks. Ieee Trans Signal Process 1997;45:2673–81.
[62] Pascanu R, Gulcehre C, Cho K, Bengio Y. How to construct deep recurrent neural networks. arXiv preprint arXiv:13126026 2013.
[63] Peebles Jr PZ. Probability, random variables, and random signal principles. McGraw Hill Book Company; 1987.
[64] Sengur A. Multiclass least-squares support vector machines for analog modulation classification. Expert Syst Appl 2009;36:6681–5.
[65] Bottou L. Large-scale machine learning with stochastic gradient descent. Proceedings of COMPSTAT'2010; 2010. p. 177–86.
[66] Bulik M, Jancalek R, Vanicek J, Skoch A, Mechl M. Potential of MR spectroscopy for assessment of glioma grading. Clin Neurol Neurosurg 2013;115:146–53.
[67] Rand S, Prost R, Haughton V, Mark L, Strainer J, Johansen J, et al. Accuracy of single-voxel proton MR spectroscopy in distinguishing neoplastic from nonneoplastic brain lesions. Am J Neuroradiol 1997;18:1695–704.
[68] Ding H, Guo L, Zhao C, Wang F, Wang G, Jiang Z, et al. RFnet: automatic gesture recognition and human identification using time series RFID signals. Mob Netw Appl 2020;1–14.
[69] Selvaraju RR, Cogswell M, Das A, Vedantam R, Parikh D, Batra D. Grad-cam: visual explanations from deep networks via gradient-based localization. Proceedings of the IEEE International Conference on Computer Vision; 2017. p. 618–26.
[70] Li Y, Yang H, Li J, Chen D, Du M. EEG-based intention recognition with deep recurrent-convolution neural network: performance and channel selection by Grad-CAM. Neurocomputing 2020;415:225–33.
[71] Majós C, Julià-Sapé M, Alonso J, Serrallonga M, Aguilera C, Acebes JJ, et al. Brain tumor classification by proton MR spectroscopy: comparison of diagnostic accuracy at short and long TE. Am J Neuroradiol 2004;25:1696–704.
[72] Luts J, Heerschap A, Suykens JA, Van Huffel S. A combined MRI and MRSI based multiclass system for brain tumour recognition using LS-SVMs with class probabilities and feature selection. Artif Intell Med 2007;40:87–102.
[73] González-Navarro FF, Belanche-Muñoz LA. Using machine learning techniques to explore 1H-MRS data of brain tumors. 2009 Eighth Mexican International Conference on Artificial Intelligence; 2009. pp. 134–9.
[74] Dimou I, Tsougos I, Tsolaki E, Theodorou K. Classification of pathological human brain lesions using magnetic resonance spectroscopy at 3T. World congress on medical physics and biomedical engineering. Munich, Germany: Springer; 2009. p. 1368–70. September 7-12, 2009.
[75] Lu D, Sun Y, Wan S. Brain tumor classification using non-negative and local non-negative matrix factorization. 2013 IEEE International Conference on Signal Processing, Communication and Computing (ICSPCC 2013); 2013. pp. 1–4.
[76] Wang L, Wan S, Sun Y, Zhang B, Zhang X. Automatic classification of brain tumor by in vivo MRS data based on LDA and SVM. 2015 Seventh International Conference on Measuring Technology and Mechatronics Automation; 2015. pp. 213–6.